The results of researching show that for bulk composition estimating is necessary to set concrete thermal model or set heat flow limitations on the crust-mantle boundary.

By this part of work following conclusions can be done:

1. Temperature distribution in mantle of the Moon essentially influence on bulk composition of silicate Moon, in the first place on concentration Al_2O_3
2. The Moon is zonal stratified by composition.
3. Silicate Moon is essentially concentrated by oxide FeO (10,5-13 mas. %) and depleted by MgO (28,5-32,5 mas.%) in comparison with earth's mantle. Magnesia number lies in the range of 0,82-0,84

References

1. V.A. Kronrod, O.L. Kuskov (2007). Modeling of thermal structure in continental lithosphere. Phisika Zemli, N1, pp. 96-107.
2. O.L. Kuskov, V.A. Kronrod (1998). Model of chemical differentiation of the Moon. Petrologia, V.6,pp. 615-633.
3. O.L. Kuskov, V.A. Kronrod (2009). Geochemical constraints on the model of composition and heat regime of the Moon according to seismic data. Phisika Zemli, N 9, pp.25-40.
4. V.A. Kronrod, O.L. Kuskov (1999). Profiles of temperature and rates of elastic waves for the model of chemically differentiated Moon. Geokhimia, N8, pp. 804-812.
5. V.A. Kronrod, O.L. Kuskov (1997). Determination of chemical composition, temperature and radius of the Moon core from geophysical data. Geokhimia, N2, pp.134-142.
6. V.A. Kronrod, O.L. Kuskov (1999). Temperature in the Moon mantle according to seismic data. Phisika Zemli V. 35, N5, pp. 363- 371.
7. Kuskov O.L., V.A. Kronrod, L.L. Hood (2002), Geochemical constraints on the seismic properties of the lunar mantle, *Phys. Earth Planet. Inter, Vol. 134*, pp. 175-189
8. McDonough W.F. (1995), Sun S.-s. The composition of the Earth, *Chem. Geol., Vol. 120*, pp.23-253

Kronrod V.A., Kuskov O. L. Chemical boundary of the cratonic lithoshere from the geophisycal and petrological data

Vernadsky Institute of Geochemistry and Analytical Chemistry, Russian Academy of Sciences, Moscow, Russia, e-mail:va_kronrod@mail.ru

Key words: Earth's mantle, craton, composition, temperature, lithosphere–asthenosphere boundary

1. **Introduction.** The lithosphere–asthenosphere boundary (LAB) represents the base of the Earth's lithosphere, the rigid and relatively cool outer shell characterised by a conductive thermal regime, isolated from the convecting asthenosphere. The lithosphere is underlain by a weak layer (the asthenosphere), which is characterised by pervasive plastic deformation (solid-state creep) on time scales of tens of thousands of years. The lithosphere is composed of discrete plates and the lithosphere–asthenosphere boundary (LAB) separates each plate from the underlying convecting mantle. The continental crust and underlying subcontinental lithospheric mantle (SCLM) are highly heterogeneous. The ranges in thickness of the lithosphere are from a few tens of kilometers beneath rift zones, to >250 km beneath some Archean cratons. Chemically, the LAB should divide a lithospheric mantle that is variably depleted in basaltic components from a more fertile asthenosphere. In xenolith suites from cratonic areas, the bottom of the depleted lithosphere is marked by a rapid downward increase in elements such as Fe, Ca, Al, Ti, Zr and Y, and a rapid decrease in the median Mg# of olivine. The petrologic (PLAB), based on xenolith and xenocryst data, thermal boundary (TLAB), based on termobarometry data and thermal physics models; the rheological LAB, based on numerical modelling of mantle creep and stress regime; the seismological LAB, based mainly on studies of surface waves and S-receiver functions; and the electrical LAB, based on magnetotelluric surveys are discussed.

In the present paper, using physicochemical modeling methods, we adjust thermal boundary layer and petrologic lithosphere-asthenosphere boundary layer of the lithosphere Archean Kaapvaal and Siberian craton. Petrologycal LAB is calculated under the assumption of local isostatic equilibrium with the compensation depth at the base of the numerical domain. According to the principle of isostasy, all regions of the Earth with identical elevation must have the same buoyancy when referenced to a common compensation level. In order to estimate absolute elevation one needs to perform a density $\rho(H)$ for the craton and reference column. With the help of physicochemical modeling methods, bulk composition models can be converted into equilibrium phase assemblages and the related seismic and density characteristics (the forward problem), while the velocity structures can be converted into composition and/or temperature distribution models (the inverse problem) [Kronrod and Kuskov, 2007, 2010]. Based on the method developed in [Kuskov et al., 2006], we reconstructed the temperature of the lithosphere at depths of 70–300 km from the composition of xenoliths from kimberlite pipes of the craton and absolute values of *P* and *S* wave velocities. The forward and inverse problems are solved by the minimization of the Gibbs free energy and equations of state of mantle material incorporating phase transformations, anharmonicity (thermal expansion and compressibility), and attenuation effects (anelasticity of mantle material at high temperatures), which should be taken into account due to nonlinear variations in thermodynamic and seismic properties with rising temperature and pressure. Equilibrium compositions of phase assemblages, elastic wave velocities, and density were calculated with the use of the THERMOSEISM software complex [Kuskov et al., 2006, Kuskov and Kronrod, 2007].

The thermal structure of continental lithosphere (the thickness of the thermal lithosphere, temperature, heat flows, and heat generation in the crust and lithosphere) is reconstructed from geothermal, seismic, and petrologic data. The first step is the determination of the temperature profile from absolute wave velocities (T_S). The T_S profile is then adjusted to a thermophysical model of conductive transfer. A feature inherent in the solution of the thermophysical inverse problem obtained in this paper is the use of constraints derived from the temperature reconstruction by seismic data inversion. As a result, the analytical dependence of the temperature on depth, the intensity of radiogenic heat sources in the crust, and heat flow components in the crust and lithosphere are determined. Profiles of the density, temperature, wave velocity in the craton lithosphere and the petrologic PLAB and thermal boundary are constructed. The results are compared with data of seismology, petrology, thermal models, and thermobarometry.

2. **Input data and method of solution.** The equilibrium composition of phase assemblages, seismic velocities, and density (a forward problem) are calculated with the help of the THERMOSEISM software package [Kuskov et al., 2006, Kuskov and Kronrod, 2007], whose database contains internally consistent values of such thermodynamic parameters as enthalpy, entropy, heat capacity, the Gruneisen parameter, thermal expansion, bulk and shear moduli of minerals, and mixing parameters of solid solutions. The model system NaTiCFMAS includes the following phases: plagioclase, Fe–Mg olivine, ilmenite, and spinel; pyrope–almandine–grossular garnet; and orthopyroxene and clinopyroxene (five- and six-component solutions). The chemical composition of the phases and their percentages are determined by the minimization of the Gibbs free energy. The equation of state of the minerals is calculated in the quasiharmonic Mie–Gruneisen–Debye approximation [Kuskov et al., 2006]. Hence, we determine the density and the isotropic velocities of the phase assemblage, which depend on the chemical and phase composition of rocks; the bulk modulus and the density are estimated from the equation of state, whereas a linear dependence is adopted for the shear modulus; and the elastic moduli are determined by the Voigt–Reuss–Hill averaging. The database contains self-consistent data on such thermodynamic parameters as the enthalpy, entropy, heat capacity, Gruneisen parameter, thermal expansion, and bulk and shear moduli of minerals and on mixing parameters of solid solutions. The model multisystem (NaTiCFMAS) includes the following phases: plagioclase, Fe–Mg olivine, ilmenite, and spinel; pyrope–almandine–grossular garnet; and ortho- and clinopyroxene (five- and six-component solutions).

The method of reconstructing the temperature from seismic information is described in detail in [Kronrod and Kuskov, 2007; Kronrod and Kuskov, 2010]. The procedure for converting seismic profiles into thermal profiles in the NaTiCFMAS multisystem with phases of a variable composition is based on the equations of state of mantle material taking into account phase transformations, anharmonicity, and anelastic effects. The temperature profiles (T_S) consistent with thermodynamic properties of minerals and the phase composition of the mineral assemblage at a given depth are determined by inverting absolute velocities with a fixed bulk rock composition. The inversion is based on the minimization of standard deviations of calculated seismic velocities adjusted to the state diagram (and corrected for anharmonicity and anelasticity) from their observed values. The minimization is performed by the Newton method. As a result of the inversion, we find a temperature–depth profile and an equilibrium phase composition of the mineral assemblage (percentages of phases and their chemical compositions) under given *P–T* conditions. The depth dependence of pressure is taken from the global PREM model.

The seismic profile was inverted on the basis of low and high temperature xenoliths from kimberlite pipes of the craton. Thus, regardless of the composition of deep xenoliths of the Kaapvaal and Siberian craton, the temperature reconstruction from the seismic velocity profiles in the regional models [Simon et al., 2002] and [Pavlenkova and Pavlenkova, 2006], leads to a temperature inversion at depths of 70-300 km. On the basis of the methods of determining the temperature in the lithosphere from seismic data (*TS*) and the 1-D model of heat conduction (*T*cond), we formulate the following inverse problem. Using the surface heat flow and the *TS* temperature profile, we have to determine the TLAB, heat generation in the upper crust, middle crust, heat flows in the crust and lithosphere. This problem is solved by minimizing a functional *f* characterizing the misfits between the temperature profile *TS* derived from seismic data and the temperature profile *T*cond calculated from model of heat conduction [Kronrod and Kuskov, 2007].

We are used reference column at a mid-oceanic ridge (MOR) [Afonso et al., 2008], where average elevations, petrogenetic processes, and lithospheric structures are known in greater detail than in any other tectonic setting, and are obtained absolute elevation are similar to those of [Afonso et al., 2008].

3. **Results.** Here, we present the results of estimating the lithosphere–asthenosphere boundary and thermal boundary layer. The chemical composition of the petrological models are listed in the Table 1, 2 in recalculation to the NaTiCFMAS system [Afonso et al., 2008, Gregoirea et al., 2005, Griffin et al., 2003, McDonough et al., 1990, McDonough and Sun, 1995]. The K1, K2 petrological models for the Kaapvaal craton, K1, K2, C for Siberian craton and P model for regions Early and Middle Proterozoic are used. Temperature of the regions Early and Middle Proterozoic we are finded from the temperature at the depths 50, 100, 150 km and surface heat flow according to [Artemieva, 2006]. Temperature profiles, values of crustal radiogenic heat sources, and heat flow components in the crust and mantle are determined. Table 2 show our reconstructions of the petrological models, petrologic lithosphere–asthenosphere boundary (PLAB) and thermal boundary (TLAB) in comparison with thermobarometric data.

4. **Conclusions.** In the present paper we adjust thermal boundary layer and petrologic lithosphere-asthenosphere boundary layer of the lithosphere Archean Kaapvaal craton and Siberian craton using physicochemical modeling methods. Petrologycal lithosphere-asthenosphere boundary is calculated under the assumption of local isostatic equilibrium with the compensation depth at the base of the numerical domain. A specific feature of the method developed for solving the inverse thermophysical problem is the incorporation of constraints obtained from the seismic data inversion for the reconstruction of temperature. The input data are seismic velocities, surface heat flows, and the petrologic models. The solution is based on the fitting of the temperature profiles derived from seismic velocities to the conductive model of heat transfer in the crust and lithosphere. The procedure of converting seismic profiles into thermal ones is based on the equations of state of mantle material taking into account phase transformations and anharmonicity and anelasticity effects. Our modeling results show good agreement with modern petrological and geothermal models.

Table 1. The chemical composition of the petrological models (wait %) in recalculation to the NaTiCFMAS system

Chemical composition	SiO_2	TiO_2	Al_2O_3	FeO	MgO	CaO	Na_2O
Garnet peridotites[a] (GP) McD 1990	45.42	0.08	1.32	7.03	45.28	0.78	0.09
Primitive Mantle[b] (PM) McD 1995	45.2	0.2	4.51	8.13	37.6	3.6	0.36
Garnet lherzolite (Daldyn)[c] (GL) Grif 2003	46.15	0.05	1.21	6.55	45.25	0.71	0.08
Coarse-grained garnet peridotites (Premier) [d] (CGP) (GR 2005)	46.23	0.08	1.64	6.83	44.12	0.98	0.12
Coarse-grained spinel peridotites (Premier)[d] (CSP) (GR 2005)	45.32	0.03	1.27	6.97	45.55	0.77	0.09
High-T lherzolite (Kaapvaal)[e] (HTL)(Af 2008)	44.76	0.17	1.76	8.17	43.74	1.28	0.12
Protons (mean garnet SCLM+massiv xenoliths) [c](P) (Grif 2003)	45.0	0.07	1.91	8.1	43.1	1.7	0.12

Note: [a] composition of [McDonough, 1990]; [b] composition of [McDonough and Sun, 1995]; [c] composition of [Griffin et al., 2003]; [d] composition of [Gregoirea et al., 2005]; [c] composition of [Afonso et al., 2008].

Table 2. Petrological models, petrologic (PLAB) and thermal (TLAB) lithosphere–asthenosphere boundary

Region	Kaapvaal craton		Siberian craton			Early Proterozoic	Middle Proterozoic
Petrological model	K1	K2	K1	K2	C	P	P
0 – Moho[a]	34 km crust	34 km crust	40 km crust	40km crust	40km crust	37.7km crust	39.3km crust
Moxo – PLAB	GP	-------	GP	-------	GL	P	P
PLAB +10 – 400 km	PM	-------	PM	--------	------	PM	PM
Moxo – 75 km	-------	CSP	-----	CSP	-------	------	------
80 km – PLAB	---------	CGP	-----	CGP	-------	-------	-------
PLAB - PLAB + 35km	-------	HTL	--------	HTL	HTL	------	-------
PLAB + 35 – 400 km	---------	PM	-------	PM	PM	-------	-------
Petrologic lithosphere–asthenosphere boundary (computing), km	173	160	210	205	197	155	110
Lithosphere–asthenosphere boundary (termobarometry[b]), km	~ 170		~190-205			~150	-----
Thermal boundary layer (computing), km	220		300			186	165

Note: The chemical composition of the petrological models GP, GL, CSP,CGP, HTL, PM, P according to Table 1;[a] Density and thickness of the crust according to [Afonso et al., 2008, Artemieva, 2006]; [b] Petrologic lithosphere–asthenosphere boundary according to [O'Reilly, Griffin, 2006, Griffin et al., 2003].

Acknowledgements

This research was supported by Russian Academy of Sciences under Programs 25, and by RFBR (grant 09-05-00254 and 09-05-00115).

References

1. Afonso J. C., M. Ferna'ndez, G. Ranalli, W. L. Griffin, J. A. D. Connolly (2008), Geophysical-petrological modeling of the lithosphere, *Geochemistry Geophysics Geosystems, V. 9*, № 5, doi:10.1029/2007GC001834.
2. Artemieva I.M. (2006), Global 1°.1° thermal model TC1 for the continental lithosphere: Implications for lithosphere secular evolution, *Tectonophysics, V. 416*, p. 245–277.
3. Gregoirea M.,T, C. Tinguelya, D.R. Bellb, A.P. le Roexc (2005), Spinel lherzolite xenoliths from the Premier kimberlite (Kaapvaal craton, South Africa): Nature and evolution of the shallow upper mantle beneath the Bushveld complex, *Lithos,V. 84*, p. 185-205.
4. Griffin W.L., S.Y. O'Reilly, N. Abea, S. Aulbach, R.M. Davies, N.J. Pearson, B.J. Doyle, K. Kivid (2003), The origin and evolution of Archean lithospheric mantle, *Precambrian Research, V. 127*, p. 19–41.
5. Kronrod V. A. and O. L. Kuskov (2007), Modeling Thermal Structure of Continental Lithosphere, *Izvestiya, Physics of the Solid Earth, 2007, Vol. 43*, No. 1, pp. 91–101.
6. Kronrod V.A., O.L. Kuskov, and A.A. Prokof'ev (2010), Temperature Distribution in the Lithospheric Mantle of the Siberian Craton: Evidence from Regional Seismic Models, *Geochemistry International, 2010, Vol. 48*, No. 8, p. 801–807.
7. Kuskov O.L., V.A. Kronrod, H. Annersten (2006), Inferring upper-mantle temperatures from seismic and geochemical constraints: Implications for Kaapvaal craton, *Earth Planet. Sci. Lett. V. 244*, p. 133-154.
8. Kuskov O.L., V.A. Kronrod (2007), Composition, temperature, and thickness of the lithosphere of the Archean Kaapvaal Craton, *Izvestiya. Phys. Solid Earth.,V. 43*. p. 42-62.
9. McDonough W. F. (1990), Constraints on the Composition of the Continental Lithospheric Mantle, *Earth Planet. Sci. Lett. V.101*, p.1-18.
10. McDonough, W. F., and S. Sun (1995), The composition of the Earth, *Chem. Geol., V.120*, p. 223–253.O'Reilly S.Y., W.L. Griffin (2006), Imaging global chemical and thermal heterogeneity in the subcontinental lithospheric mantle with

garnets and xenoliths: Geophysical implications, *Tectonophysics, V. 416*, p. 289–309.

11. Pavlenkova G. A. and N. I. Pavlenkova (2006), Upper Mantle Structure of the Northern Eurasia from Peaceful Nuclear Explosion Data, *Tectonophysics V.416*, p. 33-52.
12. Simon R.E., C. Wright, E.M. Kgaswane, M.T.O. Kwadiba (2002), The P wave speed structure below and around the Kaapvaal craton to depths of 800 km, from travel times and waveforms of local and regional earthquakes and mining-induced tremors, *Geophys. J. Int., V. 151*, p. 132-145.

Prokofyev A.A., Kuskov O.L., Kronrod V.A. Modelling of thermal mode for siberian craton by inversion of seismic profiles "rift" and "meteorite"

GEOKHI RAS, irishrover@yandex.ru cell: (915) 183-90-73

key words: litosphere, anelasticity, seismic velocities, craton

Temperature of the bowels of the earth is one of the most indefinite physical parameters. As seismic velocities are more sensitive to the temperature then to the composition, so the inversion of seismic profiles into thermal models is one of the most perspective way for estimation of the thermal field.

On constructing the seismic models all researchers have a problem with quality control of their results, because nobody knows the exact meaning of seismic velocities that can more accurately describe the features of the Earth structure. Seismic data obtained from the raw material by superlong seismic profiles survey within Siberian Craton was processed by different science groups [*Oreshin et al.*, 2002; *Pavlenkova* and *Pavlenkova*, 2006; *Egorkin*, 1999]. All velocity models differ from each other by structure and absolute values of seismic velocities. According to geodynamics, variation 0.2 km/sec in longitudinal velocity leads to temperature alteration about 500°C. Thermal profiles obtained by velocity inversion is the way to estimate the quality of each seismic model.

The main target of this research is to reconstruct the composition and thermal mode for archean mantle of Siberian Craton. Our initial data is compositions of garnet peridotite and fertile primitive mantle, also we use seismic velocities [*Pavlenkova* and *Pavlenkova*, 2006], thermobarometry [*Griffin et al.*, 1996] and heat-flow research [*Aremieva* and *Mooney*, 2001].

We must estimate the influence of chemical composition to seismic velocity and density and compare processed data with P-T valuations and thermal models. Calculation executes by minimization of Gibbs-energy in system Na_2O-TiO_2-CaO-FeO-MgO-Al_2O_3-SiO_2. P-velocities depend on P-T-X conditions, effects of phase-transformations, anharmonicity and inelasticity. To make an adjustment for inelasticity we estimate Q-factors: Q_S and Q_P.

For the composition of Siberian Craton we set a model of garnet peridotite (GP) for the depth less than 180 km and primitive mantle (PM) for more than 180 km [*Kuskov et al.*, 2011]. Deviations in velocities for GP and PM are small - 0.3% for V_P and 1% for V_S, so geotherms received from seismic models vary within 50°C [*Kuskov et al.*, 2011]. Difference in composition has a little small influence to seismic velocities and can't be registered by seismic methods [*Kuskov et al.*, 2006; *Kuskov et al.*, 2011], but it leads to increasing of density (fig. 1). The density of fertile primitive mantle is more than density of garnet peridotite at about 2-3%, that is equal to temperature deviance at 500°C.

We process two profiles – "Meteorite" (fig. 2) and "Rift" from the seismic model of N.I. Pavlenkova [*Pavlenkova* and *Pavlenkova*, 2006].

On figs 3 and 4 appears the distinction of temperatures and densities for different composition models. Comparing the permanent (GP) and variable (less than 180 km – GP, more than 180 km - PM) composition it appears, that difference in temperatures is small, but density of variable composition is more correct. On depth 210-300 km density of GP-PM model (3.42-3.49 g/cm^3) is closer to mantle density (3.426 - 3.486 g/cm^3) according to reference-model AK135 [*Kennett et al.*, 1995]. Density of GP on the same depth (3.40-3.42 g/cm^3) is obviously less than surrounding rock.

Also we determine the depth of the thermal lithosphere bound. Thermal lithosphere bound, where heat transfer accomplishes in conductive way, may be identified by finding intersections between adiabat 1200-1300°C with gradient 0.3-0.5°C/km and calculated temperature profile.

We use adiabat 1300°C and gradient 0.465°C/km. Obtained intersections describes the depth of the thermal lithosphere bound on every section of our profiles. Calculated depths was marked on 2D thermal distribution (figs. 5, 6)

Thereby the depth of the thermal lithosphere of Siberian Craton for researched profiles is very close to 1450°C isotherm and is estimated as 310-330 km that conforms with estimation by heat-flow[*Aremieva* and *Mooney*, 2001] and tomographic models [*Bijwaard et al.*, 1998].

References

1. Oreshin S., L. Vinnik, L. Makeyeva, G. Kosarev, R. Kind and F. Wentzel (2002), Combined analysis of SKS splitting and regional P traveltimes in Siberia, *Geophys. J. Int., Vol. 151*, pp. 393–402.
2. Pavlenkova G.A., N.I. Pavlenkova (2006), Upper mantle structure of the Northern Eurasia from peaceful nuclear explosion data. *Tectonophysics. Vol. 416*, pp. 33–52.
3. Egorkin, A.V. (1999), Study of the Mantle on Super Long Geotraverses, *Izv.Phys. Earth (Engl. Transl.), Vol. 35*, Nos. 7–8, pp. 630–645].
4. Griffin, W.L., F.V. Kaminsky, C.G. Ryan, et al. (1996), Thermal State and Composition of the Lithospheric Mantle beneath the Daldyn Kimberlite Field, Yakutia, *Tectonophys., Vol. 262*, pp. 19–33.
5. Artemieva, I.M. and W.D. Mooney (2001), Thermal Thicknessand Evolution of Precambrian Lithosphere: A Global Study, *J. Geophys. Res., Vol. 106*, pp. 16387–16414.
6. Kuskov O.L., V.A. Kronrod, A.A. Prokof'ev (2011), Thermal Structure and Thickness of the Lithospheric Mantle Underlying the Siberian Craton from the Kraton and Kimberlit Superlong Seismic Profiles, *Izv.Phys. Earth (Engl. Transl.), Vol. 147*, No. 3, pp. 155–175.
7. Kuskov, O.L., V.A. Kronrod (2006), Determining the Temperature of the Earth's Continental Upper Mantle from Geochemical and Seismic Data, *Geochem. Int. (Engl. Transl.)*, no. 3, pp. 232–248.
8. Kennett B.L.N., E.R. Engdahl, R. Buland (1995), Constraints on seismic velocities in the earth from travel times, *Geophys. J. Int, Vol. 122*, pp. 108-124
9. Bijwaard H., W. Spakman, E.R. Engdahl (1998), Closing Gap between Regional and Global Travel Time Tomography, *Geophys. Res., Vol. 103*, pp. 30055–30078.

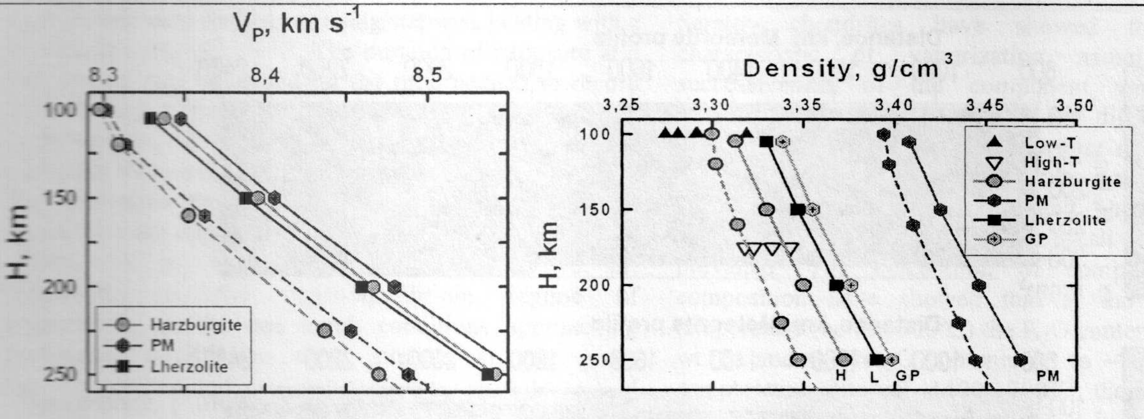

Fig. 1. P-velocities and densities along geotherms 35 (solid lines) and 40 mW/m^2 (dashed lines). Velocities of depleted matter are very close to primitive mantle, but density of primitive mantle is 2-3% more than density of garnet peridotite that equals ΔT about 500-700°C.

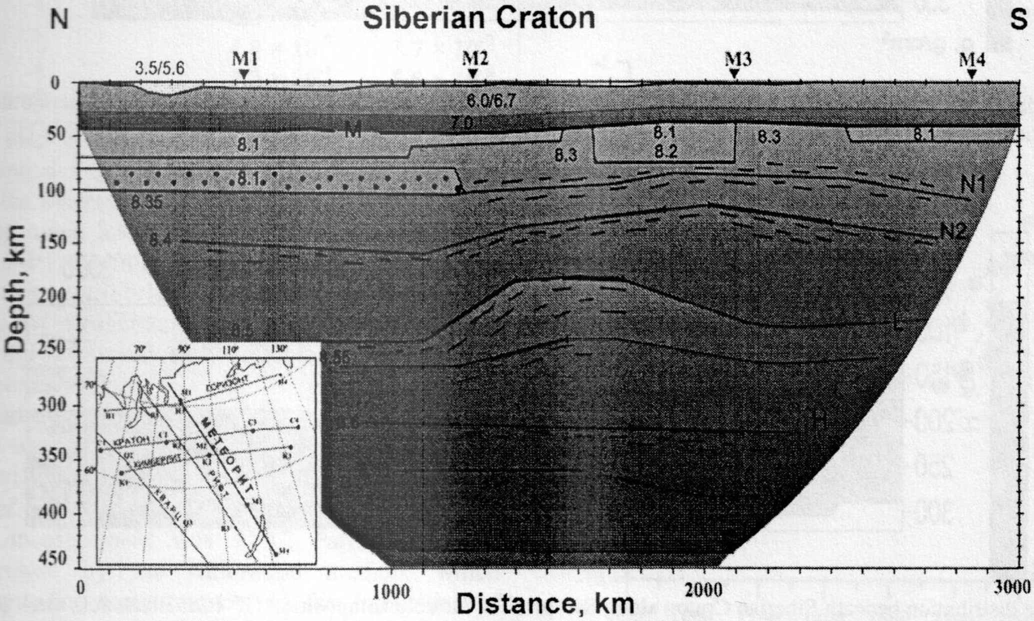

Fig. 2. Seismic velocities for profile "Meteorite" [*Pavlenkova* and *Pavlenkova*, 2006].

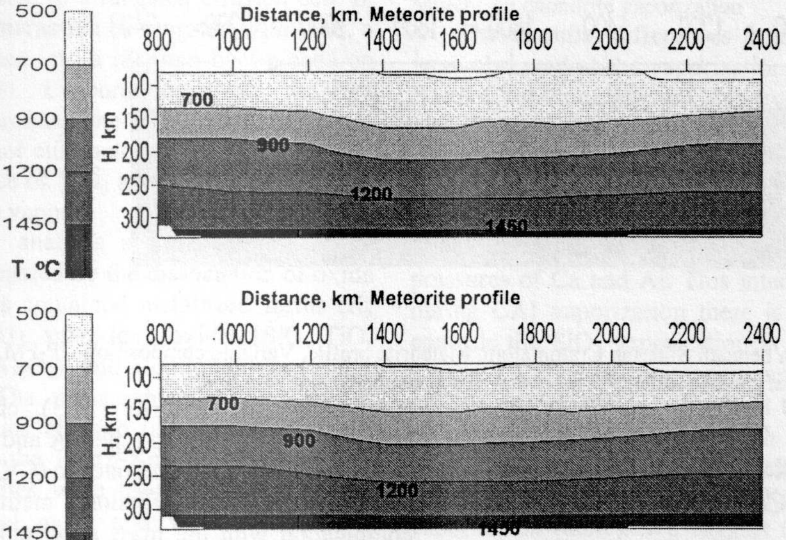

Fig. 3. Recovered temperature as a function of composition model. The upper pattern – permanent composition of garnet peridotite (GP), the lower one – variable composition (less than 180 km – GP, more than 180 km – primitive mantle (PM))

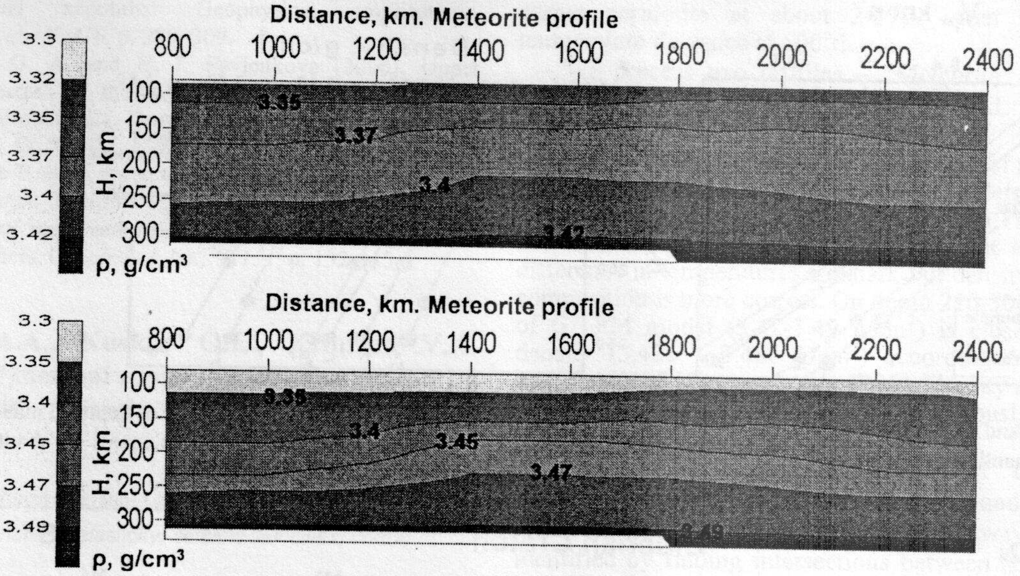

Fig. 4. Recovered density as a function of composition model. The upper pattern – permanent composition of garnet peridotite (GP), the lower one – variable composition (less than 180 km – GP, more than 180 km – primitive mantle (PM))

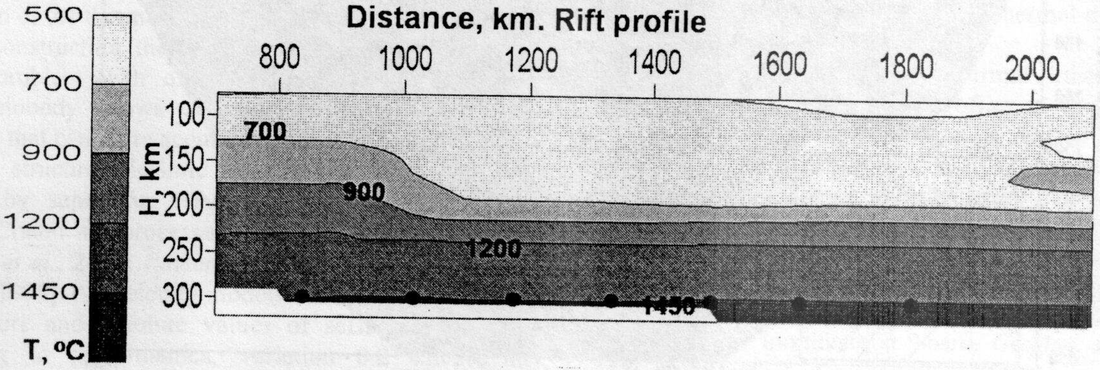

Fig. 5. Temperature distribution beneath Siberian Craton along Rift profile. Variable composition GP-PM. Black dots mark the depth of thermal lithosphere, that is close to 1450°C isotherm and is estimated as 300-320 km.

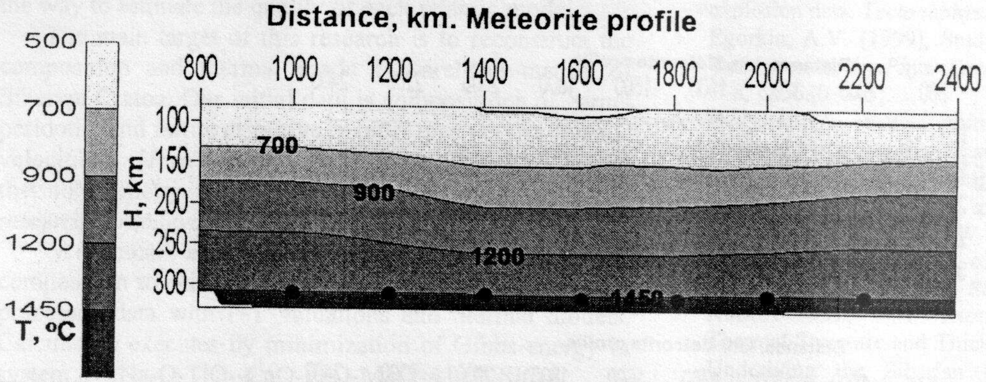

Fig. 6. Temperature distribution beneath Siberian Craton along Meteorite profile. Variable composition GP-PM. Black dots mark the depth of thermal lithosphere, that is close to 1450°C isotherm and is estimated as 310-330 km.

Yakovlev O.I., Shornikov S. I.. Experimental study of meteorites and Ca-Al-inclusions

GEOKHI RAS yakovlev@geokhi.ru

Key words: evaporation, condensation, meteorites, oxygen pressure

To study the vaporization processes of the meteorites matter there were carried out some experiments by Knudsen cell method. We vaporized: Murshison chondrite (CM), Krymka chondrite (LL3), chondruls of Saratov chondrites (L4) and two types (A and B) Ca-Al-inclusions (CAI) from Efremovka chondrite (CV).

The Knudsen effusion method was used in combination with the mass spectrometric analysis of the vapor phase (MS-1301 mass spectrometer) [***Semenov et al., 1976***]. This method allowed us to determine quasi-equilibrium parameters (temperature and partial pressures of the components) in the melt–vapor system within a wide temperature range (up to ~2600°C) and measure the partial pressures of the components at a level of 10^{-7} mm Hg. The upper pressure limit was 10^{-1} to 10^{-2} mm Hg. The experiments were carried out using stepwise heating with a temperature step of ~50°C. The duration of exposure at a temperature step depended on the time needed to record the whole mass spectrum of the sample and was ~15 min. Such stepwise heating conditions allowed maintaining the molecular regime of vapor effusion at a given sample mass and minimized the duration of experiments. The total duration of the experiment from a sample temperature of ~900°C to its complete evaporation was ~5 hr. Noteworthy is the quasi-equilibrium regime of evaporation: on the one hand, conditions approaching melt–vapor equilibrium were attained at any given temperature step in the Knudsen cell, and, on the other hand, continuous vapor flow through the effusion hole occurred in the molecular regime. Since the rate of vapor emission was much lower than the rate of equilibration, the experimental conditions allowed us to consider the evaporation as an equilibrium process, and the emission of vapor during the measurement of the partial pressures of components did not significantly affect the composition of melt and vapor.

Temperature, °C	Murchison	Efremovka, Type A	Efremovka, Type B
2020	**1.9×10^{-9}**		
2072	**2.1×10^{-9}**		
2130	**2.0×10^{-9}**	**2.7×10^{-8}**	**4.5×10^{-7}**
2180		**6.3×10^{-9}**	
2205		**4.8×10^{-9}**	**3.7×10^{-7}**
2267		**7.3×10^{-8}**	**5.5×10^{-8}**
2348		**2.5×10^{-7}**	

The Knudsen cell was heated by an electron beam. Temperature was measured using an optical pyrometer in the the pyrometric hole of the cell, which imitated the conditions of black body radiation. The accuracy of temperature measurement was ±1°C. Partial pressures were determined by the calibration method, which involved sequential measurements of the intensities of ionic currents of a standard and the material of interest occurring in the same cell. Gold was used as a standard. Evaporation was conducted in a tungsten effusion cell. In order to minimize the interaction of tungsten with melt, a 15 mg sample was loaded into a rhenium boat placed on the bottom of the cell. Evaporation in the rhenium container strongly depressed the reducing activity of tungsten, although did not eliminate it completely. This is suggested by the presence of WO_2 and WO_3, as well as Ca and Mg tungstates in the vapor.

Mass spectrometric analysis showed that the melt evaporation was accompanied by the dissociation of oxide components. The vapors contained metallized forms (K, Na, Fe, Mg, Ca, and Al), suboxides, oxides (SiO, TiO, TiO_2, AlO, Al_2O, and Al_2O_2), and atomic and molecular oxygen (O and O_2). The measurement of the partial pressures of these species allowed us to calculate their evaporation rates using the Hertz–Knudsen equation. In turn, the evaporation rates were used to determine the compositions of residual melts and vapors at various temperatures and evaporation mass losses. Temperature and mass losses are are interrelated during evaporation, but in a real process, mass loss is a rather complicated function depending on the evaporation rate of particular components at a given temperature and duration of evaporation.

The experimental results on the vaporization of Murshison chondrite, Krymka chondrite, chondruls of Saratov chondrites have showed that the main characteristic of vaporization namely temperature successiveness of the component vaporization was practically identical and it did not differ from famous basalt vaporization data [*Markova et al.*, **1986**]. In the figure 1 the experimental results on the Murshison chondrite vaporization are presented. They showed that at the initial vaporization stages the alkali components were prevailed. The calculation of complimentary vapor composition have showed that at the relatively low temperature (up to 1300°C) the K_2O contents reached 5-10 wt. % and the Na_2O contents up to ~70 wt. %. In the temperature interval 1400-1700°C the Fe vapor was prevailed and reached ~40 wt. %. It is important to note that at the temperature 1800°C and higher the SiO disappeared in the vapor phase while the Al_2O_3 and CaO increased. The Al_2O_3 contents reached 60-65 wt. % at the temperature ~2000°C.

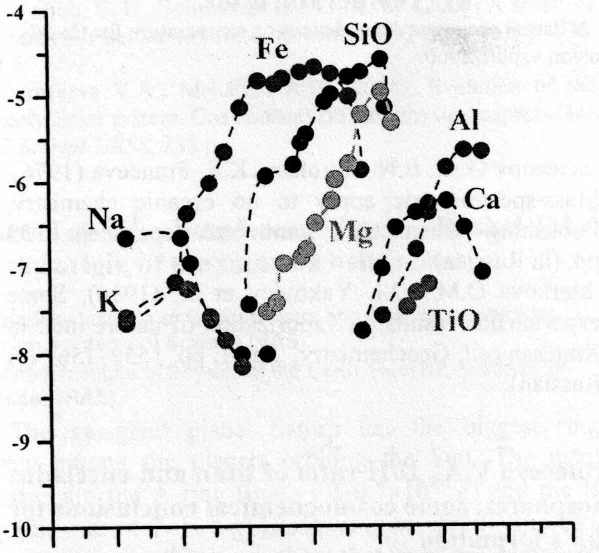

Fig. 1. Partial pressures dependences on temperature for Murchison chondrite vaporization

The essential differences from chondrite vaporization were observed at the vaporization of main types ((A and B) of Ca-Al-inclusions (CAI) from Efremovka chondrite that was shown in figure 2.

At high temperature fields (2000-2400°C) one can see the SiO form together with low fugacity components of Ca and Al. Besides the partial pressure value of SiO is rather high (~10^{-6} bar) and it is approximately equal to partial pressures of Ca and Al. This interesting result testify that during CAI vaporization there is unknown factor which controls the SiO_2 vaporization at very high temperatures (>2000°C). The thermodynamic analyses of the conditions of CAI vaporization showed that the vaporization process proceeded at comparatively high oxygen pressure which was in 10 and 100 times higher then oxygen pressure condition at the Murchison and Krymka high temperature vaporization (table). We suggest that just extremely high oxygen partial pressure decreases SiO_2 fugacity during CAI vaporization. This conclusion may be important for CAI genesis as it stresses the specific conditions for CAI vaporization/condensation and hints on its extra solar origin.

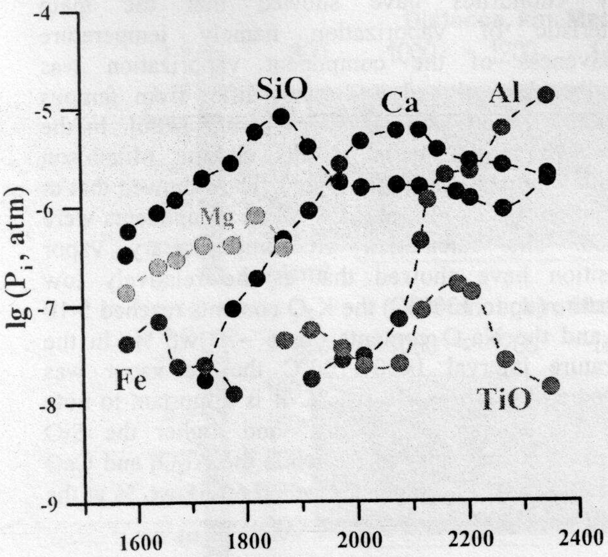

Fig. 2. Partial pressures dependences on temperature for Ca-Al-inclusion vaporization

References

1. Semenov G.A., E.N. Nikolaev, K.E. Franceva (1976), Mass-spectrometric apply to no organic chemistry, Publishing "Chemistry", Leningrad department, 152 pp. (in Russian)
2. Markova O.M., O.I. Yakovlev et al. (1986), Some experimental results on vaporization of nature melt in Knudsen cell, Geochemistry, № 11. pp. 1559–1569 (in Russian).

Dorofeeeva V.A. D/H ratio of titan and enceladus atmospheres: some cosmochemical conclusions for moon's formation

Vernadsky Institute or Geochemistry and Analytical chemistry, Russian academy of Science (dorofeeva@geokhi.ru)

«Cassini-Huygens» spacecrafts in 2005-2010 performed the detailed studies of the Saturnian moon system. The quantitative data were firstly obtained in relation to the atmospheric and isotopic composition of Titan atmosphere along with new «Cassini» discovered Enceladus aqueous plumes. It was found the Titan atmosphere consisting of only two macrocomponents: $N_2 \geq 95$ mol. % ($^{15}N/^{14}N = 5.99\times10^{-3}$) [*Owen, Niemann*, 2009] and CH_4, the latter being about 1% at 50 km altitude and as high as 5% near the moon surface [*Niemann*, 2005]. D/H ratio of molecular $CH_4 = 1.58\times10^{-4}$ [*Abbas et al.*, 2010] showed extraordinary agreement with the standard D/H value of terrestrial oceanic water = 1.56×10^{-4} (VSMOW-Vienna Standard Mean Ocean Water) as well as with D/H in hydroxile (OH^-) of carbonaceous chondrites (mean D/H value varies from 1.3×10^{-4} up to 1.7×10^{-4} [*Robert*, 2006]). At the same time D/H value in molecular hydrogen of the Enceladus aqueous plumes was found as $2.9^{+1.5}_{-0.7}\times10^{-4}$ [Waite et al., 2009] being near to D/H of five comets (from $(2.9\pm1)\times10^{-4}$ up to $(4.7\pm1.1)\times10^{-4}$ [Villanueva et al., 2009]) (Fig. 1).

It should be noted that above mentioned H_2 is interpreted as a product of H_2O molecule dissociation.

Before the «Cassini» new data were obtained, it was abundantly assumed that ice planetesimals formed in the nebula (solar gas-dust protoplanetary disc), could serve as a source of volatiles for all Jovian and Saturnian moons including Titan and Enceladus. Such planetesimals were assumed to contain rock component, H_2O and CO_2 ice as well as some other gases in a form of solid clathrates which could be formed in the process of appropriate nebular regions cooling up to temperature lower then ~ 80 K. The contemporary bulk elemental and isotopic composition of Jovian and Saturnian atmospheres could be in some sense analogous to their "ancient" composition. But in any case the relations between the main volatile elements, such as C, N, O, incorporated in various chemical compounds (NH_3:N_2; CH_4:CO:CO_2) as well as carbon fraction in the solid organic matter was remained undetectable. The clathrate composition of the ice planetesimals also was undistinguished. Some volatiles were dissipated from the Saturnian protosatellite disc (sub-nebular) but the experimental data indicating to the appropriate thermodynamical conditions are absent. All these circumstances make the problem of regular Saturnian satellite system origin to be highly complicated. New information on the hydrogen isotopic composition of Titan and Enceladus atmospheres is just very valuable in such matter.

The Titan atmosphere is characterized by the absence of heavy noble gases (Xe and Kr), as their clathrates could be formed in the protoplanetary disc only at $T \leq 60$K. This peculiarity imposes the constraints to the molecular nitrogen formation in the Titan atmosphere. It is known that nitrogen clathrate formation temperature is very low ($T \leq 40$K). Such temperatures were likely not achieved in the feeding zone" of the Titan ice-rock planetesimals, so the most probable nitrogen source in the Titan atmosphere could be only the ammonium clathrate ($NH_3 \cdot H_2O$).

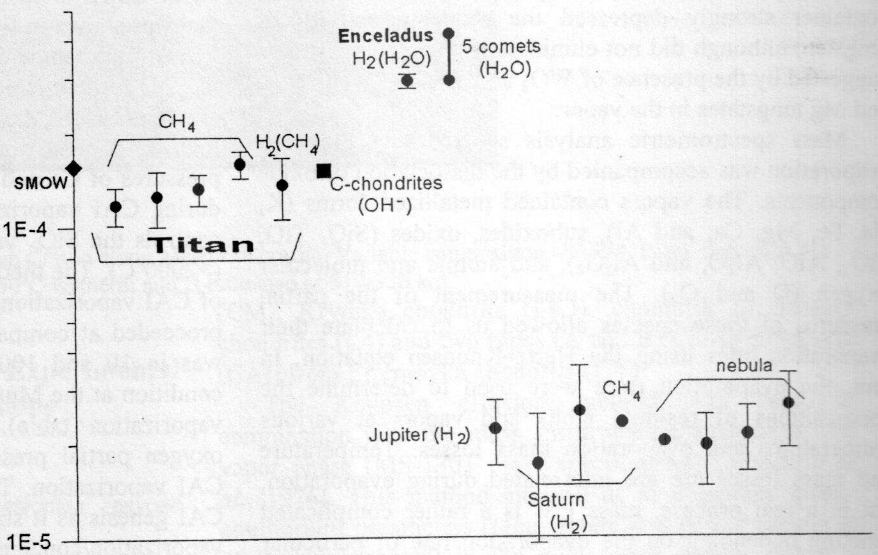

Fig. 1. D/H ratios of some Solar system objects.

The are two main hypotheses of CH_4 origin in the Titan atmosphere, the former being the second abundant atmospheric component. (1) CH_4 could be formed as the product of interaction of CO_2 dissolved in water with the hydrogen. It is assumed that CO_2 could be considered as one of probable carbon-bearing phases accreted by Titan. The hydrogen could be evolved as a product of silicate interaction with aqueous solutions (serpentinisation reaction). (2) The thermodynamical conditions of the nebula and the Saturnian sub-nebula allowed to accrete CH_4 as well as CO_2, the former being introduced to the satellite atmosphere.

The agreement of D/H values of CH_4 in Titan atmosphere with that of SMOW hardly could be occasional, thus water should be involved in methane formation, so the first version is mostly plausible and CO_2 could be assumed as a source of methane. This conclusion leads to another consequence: H_2O ice in the Solar disc (nebula) was evaporated in the space in the region up to $r \sim 10$ A.U. if even not to longer radial distances. It could be very probable that D/H values in water molecules primarily being near to the comet ratios varied as a result of isotopic exchange with the molecular hydrogen, the isotopic composition of the latter being near to the Jovian (Fig. 1). As a result the newly detected D/H values are peculiar of the inner planetary regions ($r \leq 10$ A.U.). This conclusion could be supported by the computer modeling of the protoplanetary disc inner structure (Dorofeeva, Makalkin, 2004). According to this study water existed in gaseous phase even at the Saturnian radial distance as a product of the probable proceeding of the reaction:

$$HDO + H_2 = H_2O + DH$$

H_2O ice incorporated in Enceladus was presumably not evaporated, thus Enceladus was presumably formed not within the Saturnian protosatellite disc but in the Solar nebula at the radial distances above 10-15 A.U.. The temperature of this region was substantially lower, so the Enceladus could be accrete some more fugitive gases than H_2O and CO_2 in a form of clathrates. The absence of Kr and Xe in the Enceladus water plumes is highly surprising and it is difficult to explain this phenomenon.

New «Cassini-Huygens» data on the hydrogen isotopic composition of the Titan atmosphere and Enceladus water plumes are compared with the analogous information on CI-chondrites, SMOW value, comets, Jovian and Saturnian atmospheres. It is shown that H_2O molecules could be considered as the most probable hydrogen source of the Titan atmospheric CH_4 and the Enceladus water plumes. This water probably was accreted in a form of ice in the process of proto-satellite body formation. We assume that the Enceladus water ice in contrast to that of Titan was formed at the radial distance above 10-15 A.U. where it could not be evaporated and accreted in the amorphous state. This conclusion was performed at the base of contemporary estimates of the characteristic time intervals of gas-dust disc evolution around the solar type stars, as well as the same values of planetesimals formation and differentiation within the outer part of the Solar nebula and models of thermal and dynamical conditions of the Saturnian sub-disc.

Acknowledgments: This work was supported by the Russian Foundation for Basic Research, Grant 11-05-01137

References

1. Abbas M.M., Kandadi H. et al. (2010), D/H ratio of Titan from observatios of the Cassini Composite infrared spectrometer, *The Astrophysical J.*, V. 708, p. 342–353.
2. Niemann H.B., Atreya S.K., Bauer S.J. et al. (2005), The abundances of constituents of Titan's atmosphere from the GCMS instrument on the Huygens probe, *Nature*, V. 438, p. 779-784.
3. Owen T., Niemann H. B. (2009), The origin of Titan's atmosphere: some recent advances, *Philosophical Transactions of the Royal Society A: Mathematical, Physical and Engineering Sciences,* V. 367, iss. 1889, pp. 607-615.
4. Robert F. Solar System Deuterium/Hydrogen Ratio (2006), *Meteorites and the Early Solar System II, D. S. Lauretta and H. Y. McSween Jr. (eds.), University of Arizona Press, Tucson*, 943 pp., p. 341-351
5. Waite J.H., Lewis W.S., Magee B.A. et al. (2009), Liquid water on Enceladus from observations of ammonia and ^{40}Ar in the plume, *Nature*, V. 460, № 7254, p. 487–490.
6. Villanueva, G. L., Mumma, M. J., Bonev, B. P., Di Santi, M. A., Gibb, E. L., Bohnhardt, H., Lippi, M. (2009) A sensitive search for deuterated water in comet 8P/Tuttle, *ApJ*, p. 690, L5
7. Dorofeeva V.A., Makalkin A.B. (2004), Evolution of the early Solar system. Cosmochemical and physical aspects, *M.: Editorial URSS*, 288 p.

Roussol A.V.[1], Dorofeeeva V.A.[1], Ruskol E.L.[2] *On* the origin of the saturn's belts matter

[1]Vernadsky Institute or Geochemistry and Analytical chemistry, Russian academy of Science (RAS)
[2] Schmidt Institute of Physics of the Earth, Russian Academy of Sciences (RAS)

The gas-giant planet Saturn has the biggest ring system among the planets orbiting the Sun. The most massive are the A ring (mass $0.5\text{-}0.7\times10^{22}$ g) and the B ring (the mass $4\text{-}7\times10^{22}$ g) [*Robbins et al.*, 2010]. The data by space mission "Cassini" show that rings are composed from particles of almost pure (95-98%) crystal water ice with dimensions 10 cm – 10 m [*Nicholson et al.*, 2008]. The problem of the origin of rings' matter has been investigated since long time. In most cases the models have usedthe idea of the disruption of a body (a comet or a satellite) that approached to Saturn inside the Roche limit, and there was disintegrated by an impact or by tidal forces of the planet. So the models [*Pollack et al.*, 1973; *Pollack,* 1975; *Harris,* 1984] are based on disruption of a satellite orbiting on Roche limit distance by an impact of a comet. In the models [*Dones*, 1991; *Dones et al.*, 2007] as the source of the rings matter a massive comet is considered which passed by Saturn on eccentric orbit and was disrupted by tidal forces. The recent model [*Canup,* 2010] suggested that a very massive Titan-like satellite was tidally disrupted. This body is supposed to be already differentiated. Its approach to Saturn is ascribed to the interaction with the spiral density waves in the gas-dust accretion disc of Saturn.

The analysis of all these models with the account of modern evidence shows that the hypothesis that comets may be main source of rings' material is very doubtful. First, cometary masses are too low for providing the mass of the Saturnian rings. Second, the comets' material is known as a fluffy (the dence 0.2-0.5 g/cm^3) mixture of the amorphous ice, the silicate dust and solid organic compounds. But the rings contain the almost pure crystal ice, and therefore, on our opinion, the more realistic would be the fragmentation of a differentiated rock-ice body in which the water ice was melted and crystallized. With the account of loss of the matter in the process of evolution, the initial mass of the ice in the body had to be at least on order of magnitude more than the mass of the rings. However the suggestion [*Canup,* 2010] that the primary body was a large Titan-like differentiated satellite seems to be too extremal (3 orders of magnitude of mass excess), the model by [*Canup,* 2010] also is related to the earliest epoch of the solar nebula (may be < 5 million yr) and that may be in contradiction with the contemporary views on the origin of the Saturnian system [*Dorofeeva, Ruskol,* 2010].

We present here a model, in which the source of icy material of rings is the icy mantle of an ice-rock body of mass 10^{23}- 10^{24} g and radius ~ 600 km which approached Saturn after the gas was already dissipated from the Solar system (including accretion disks). The body could come from the periphery of the Solar system, where even at present time exist many large bodies of Kuiper belt. The possibility of an early differentiation of similar bodies, with the separation of the silicates (~ 30% mass) was considered in [*Busarev et al.,* 2003]. There is much evidence of multiple impacts of different bodies (including large ones) which penetrated into Saturnian system and left millions of craters on satellites from Mimas ($r \sim 3R_{\mathrm{Sat}}$) to Iapetus ($r \sim 59R_{\mathrm{Sat}}$). Many small satellites of Saturn presumably are fragments of disintegrated large bodies (Telesto, Helena etc.).

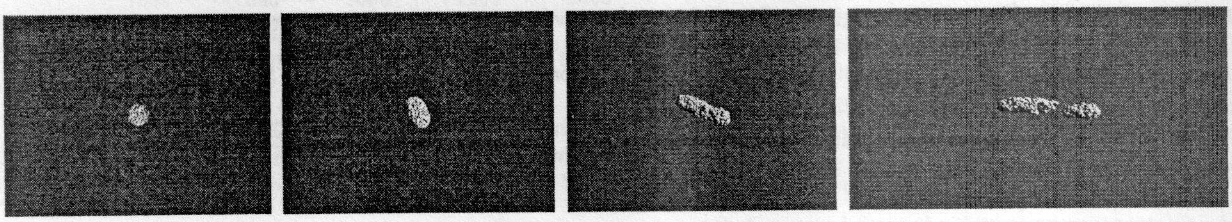

Fig. 1. Several stages of tidal disruption of a body inside the Roche limit.

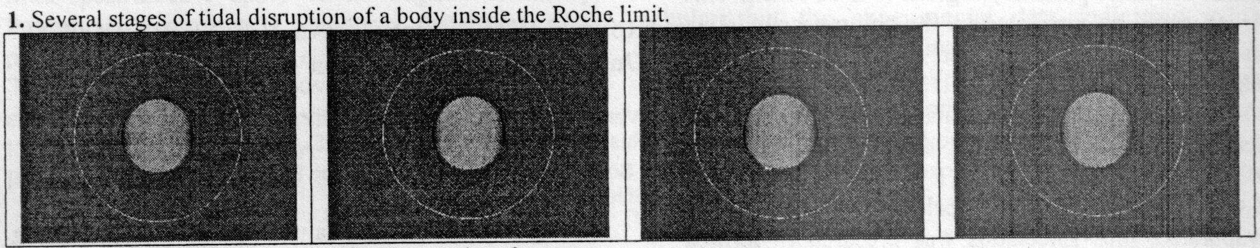

Fig. 2. Velocity of an entrance less circular for a point of an entrance

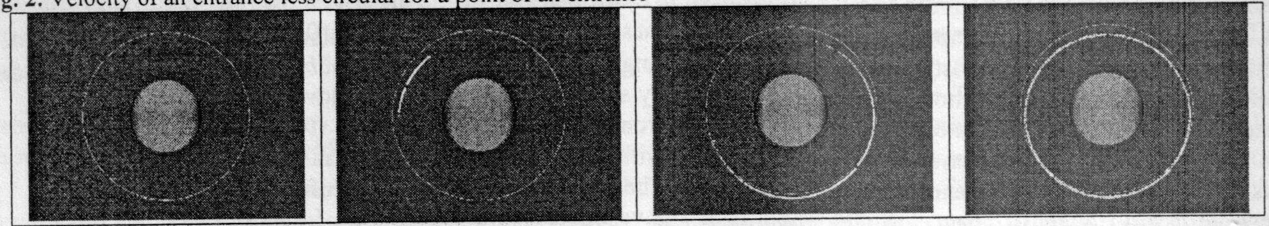

Fig. 3. Velocity of an entrance is close to circular

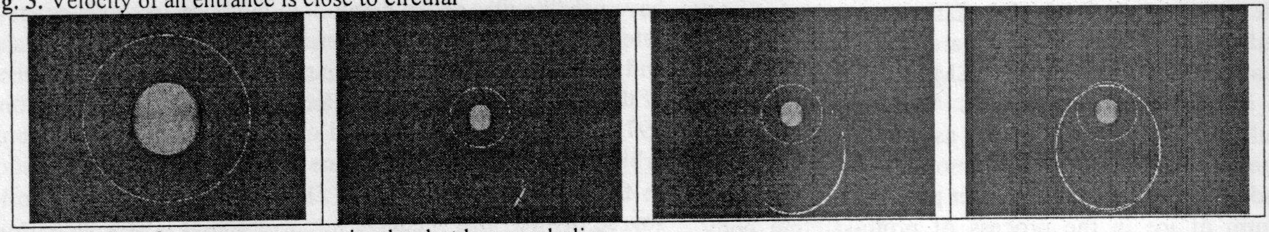

Fig. 4. Velocity of an entrance more circular, but less parabolic

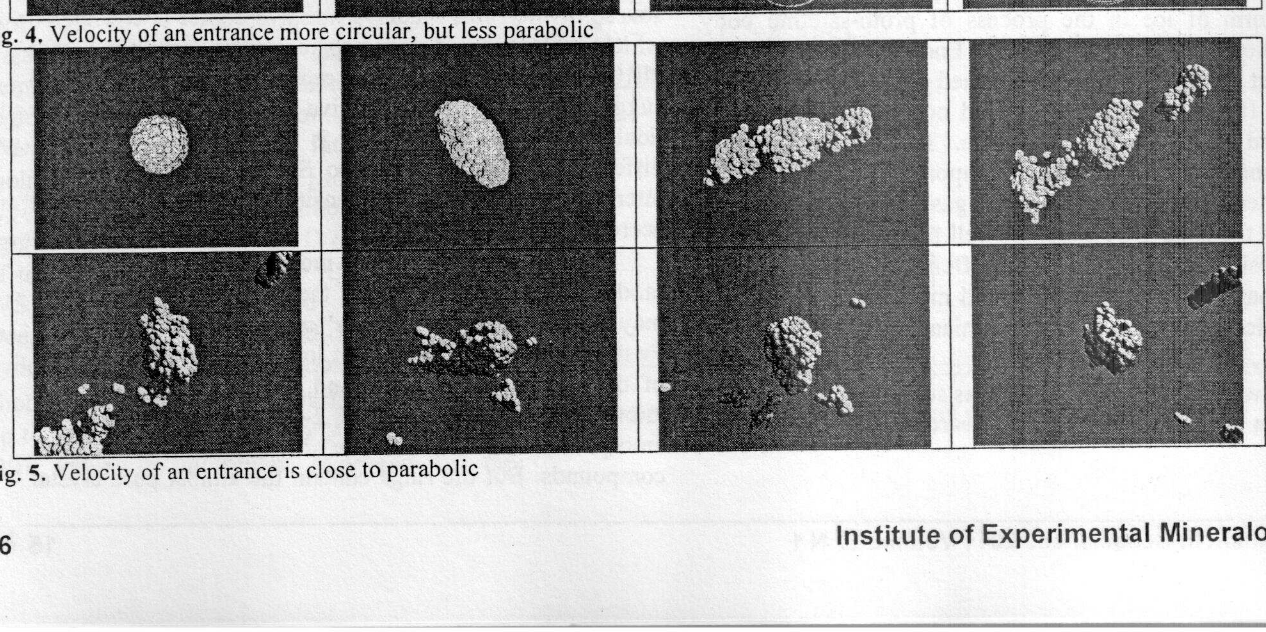

Fig. 5. Velocity of an entrance is close to parabolic

We consider as a mechanism of disruption of the body the tidal force of Saturn, acting at Roche limit distance 1.5–2.0R_{Sat} (depending on the density of approaching body). The mantle of the body undergoes a deformation and fragments as it is shown on fig. 1. To follow further behaviour of fragments we used a numerical method of penetratable particals [*Marov, Roussol*, 2011].

At realization of numerical experiments the following cases of an entrance inside the Roche limit were considered: velocity of an entrance less circular for a point of an entrance (fig. 2); velocity of an entrance is close to circular (fig. 3); velocity of an entrance more circular, but less parabolic (fig. 4); velocity of an entrance is close to parabolic (fig. 5).

Conclusions

1. The source of the icy particles of Saturn's rings could be represented a rock-ice body with radius ~ 600 km and a mass of 10^{23}- 10^{24} g, which came into zone of tidal disruption of Saturn after the dissipation of gas from Saturnian subnebula (or gas-dust accretion disk).
2. It is shown that the fragments remain on elliptic orbits around the planet if the body enters into Roche zone at the velocity between circular and parabolic ones.
3. The presents of a layer of the liquid water in the rock-ice body is favorite for its disruption, but nevertheless is not necessary in this process.
4. The fate of the rocky core of the body is not yet determined but it is possible that the fragments of the core could be transformed into shepherding satellites.

Acknowledgments: This work was supported partly by the Russian Foundation for Basic Research, Grants 08-02-00275-a and 11-05-01137

References

1. Dones, L. (1991). A recent cometary origin for Saturn's rings? *Icarus* V. 92, p. 194–203.
2. Dones, L., Agnor, C.B., Asphaug, E. (2007), Formation of Saturn's rings by tidal disruption of a Centaur, *Bull. Am. Astron. Soc.* V. 39. #7.07.
3.
4. Dorofeeva, V. A.; Ruskol, E. L. (2010), On the thermal history of Saturn's satellites Titan and Enceladus,
5. *Solar System Research*, V. 44, Iss. 3, p.192-201
6. Harris, A. (1984), The origin and evolution of planetary rings, *Planetary Rings*, Greenberg, R., Brahic, A. (Eds.), Univ. Arizona Press, Tucson, p. 641–659.
7. Kunin S. (1992), *Computing physics,* M. Mir, 518 p.
8. Nicholson P.D. Hedman M.M. et al. (2008), A close look at Saturn's rings with Cassini VIMS, *Icarus*, V. 193, p. 182–212
9. Marov M.Ya., Roussol A.V. (2011), Model of impact interaction of bodies in a gas-dust protoplanetary
10. disk, *DAN* (*Reports of an Russian academy of sciences*), in press
11. Panovko Ya.G. (1976), *Bases of the applied theory of fluctuations and impact,*L. Mashinostroenie, 320 p.
12. Pollack, J.B. (1975), The rings of Saturn, *Space Sci. Rev.*, V. 18, p. 3–93.
13. Pollack, J.B., Summers, A., Baldwin, B. (1973), Estimates of the sizes of the particles in the rings of Saturn and their cosmogonic implications, *Icarus*, V. 20, p. 263–278.
14. Robbins S.J., Stewart G.R. et al. (2010), Estimating the masses of Saturn's A and B rings from high-optical depth N-body simulations and stellar occultations, *Icarus*, V. 206, Iss. 2, p. 431-445.
15. Busarev V. V., Dorofeeva V. A., Makalkin, A. B. (2003), Hydrated Silicates on Edgeworth-Kuiper Objects - Probable Ways of Formation, *Earth, Moon, and Planets,* V. 92. Iss. 1, p. 345-375.

Alexeev V.A. Distributions of extraterrestrial and terrestrial chromite grains in ordovician limestone of Sweden and China

GEOKHI RAS AVAL37@chgnet.ru; +7(499)137-86-14

Keywords: fossil meteorites, radiation age

More then 80 fossil meteorites were recovered from mid-Ordovician marine limestone in the Thorsberg quarry in the southern Sweden. These meteorites have been identified as fragments of the L-chondrite parent body (asteroid) which was destroyed in a catastrophic collision in space ~470 Ma [*Schmitz et al.*, 1997; *Heck et al.*, 2004]. In this quarry together with meteorites, there were also found the relic sediment-disperse extraterrestrial (EC) and terrestrial (OC) chromite grains. Similar grains were also found in several correlated sediment beds of other quarries in Sweden and in China [*Cronholm, Schmitz*, 2010].

Sediment-dispersed EC grains are two orders-of-magnitude more abundant over a part, representing a few million years, of mid-Ordovician strata compared to background levels. Detection of the solar wind noble gases in EC grains (Fig. 1) has allowed to identify unequivocally and convincingly these grains as micrometeorites which have been generated as dust during the disruption of the L chondrite parent body and arrived on all Earth over a timescale of 1-2 Myr [*Heck et al.*, 2008; *Meier et al.*, 2010].

We can see on Fig. 1, the difference of ^{20}Ne content in the extraterrestrial and terrestrial chromite grains exceeds two orders-of-magnitude. The increase in the ^{20}Ne content with decrease of mass of grains is caused by increase in a specific surface of grains at decrease of their sizes. The identical inclination of the regression lines (parameter of *b* in the equation of lines, Tab. 1) is evidence of the surface-correlated mechanism of capture of gases as solar (for EC grains) and terrestrial (for OC) origins. High abundance of fossil meteorites (in the Thorsberg quarry) and relic chromite grains (in all quarries) have given the basis for the assumption, that the stream of extraterrestrial material to the Earth during several millions years ~470 Ma was, at least, on two orders of magnitude above, than now [*Schmitz et al.*, 2003; *Alwmark, Schmitz*, 2009].

However, the beds with high abundance of extraterrestrial chromite grains have high abundance and terrestrial grains also (Fig. 2). For comparison of concentration of both grain populations (EC and OC), we shall enter the factor of enrichment (K) for extraterrestrial (K_{EC}) and terrestrial (K_{OC}) grains:

$$K_{EC} = (N_{EC}/M)_{FM}/\ (N_{EC}/M)_{NFM} \text{ и } K_{OC} = \\ = (N_{OC}/M)_{FM}/\ (N_{OC}/M)_{NFM}.$$

Here N is the number of extraterrestrial (N_{EC}) or terrestrial (N_{OC}) grains found in the limestone mass of M. The FM index is related to the limestone beds equivalent with those, containing fossil meteorites. The NFM index is related to the beds that have formed during other time. N_{EC}/M and N_{OC}/M are concentration of extraterrestrial and terrestrial grains in limestone correspondingly.

Table 1. The parameters of the equation for the regression line $\lg(^{20}\mathrm{Ne}) = a + b \times \lg m$ for the dependence of the content of ^{20}Ne (10^{-8} cm^{3}g^{-1}) on the mass (m, μg) for the extraterrestrial (EC) and terrestrial (OC) individual chromite grains from the Thorsberg quarry, southern Sweden. 1)

Chromites	*a*	*b*	*R*
EC	4.14 ± 0.1	-0.93 ± 0.02	-0.77 ± 0.08
OC	1.41 ± 0.3	-1.03 ± 0.13	-0.88 ± 0.07

1) According to [*Meier et al.*, 2010].

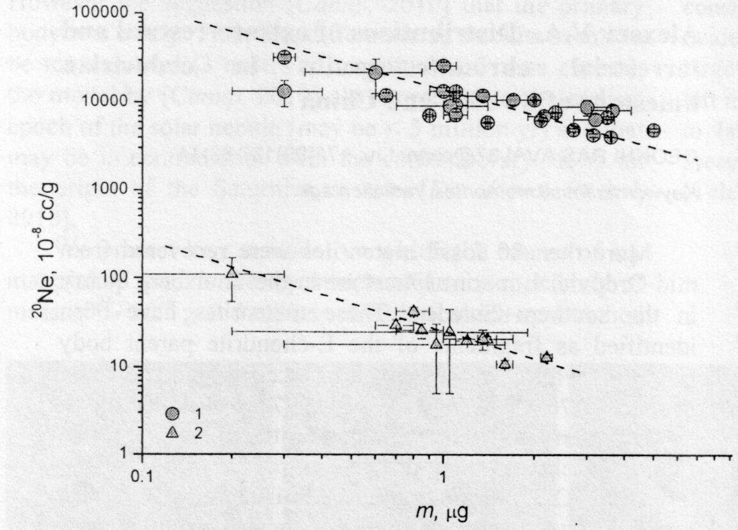

Fig. 1. Content of ^{20}Ne in individual extraterrestrial (1) and terrestrial (2) chromite grains vs. mass of grains (according to [*Meier et al.*, 2010]). Dotted lines are regression lines.

From the data shown in the Table 2, we can see, for example, the concentration of extraterrestrial grains in the Thorsberg and Hällekis quarries in the beds equivalent with those containing fossil meteorites, exceeds concentration of EC grains in the layers that have formed during other time, in 49 ± 13 times (i.e. K_{EC}=49). At the same time, the factor of enrichment for terrestrial grains is equal to K_{OC} = 28 ± 9, that within the limits of an error is in accord with K_{EC} value. (The errors were calculated as $\sigma(N) = \sqrt{N}$.) For all data set (Tab. 2) the value of enrichment by the extraterrestrial chromite grains is on average equal to 40 ± 8. However, high concentration of the OC grains (K_{OC} = 23 ± 7) in the beds with high concentration of the EC grains can testify about processes of enrichment at the bottom of the sea because of hydrodynamical sorting that especially effectively could be occurred at formation of limestone beds in Sweden [*Cronholm, Schmitz*, 2010].

Taking into consideration these data, it is apparently possible to say about increase in a stream of *micrometeorites* on all Earth after destruction of parental body L-хондритов no more than several times but not on two orders of magnitude above than now. But for all that, the high concentration of fossil *meteorites* in the south of Sweden is most probably caused by fall of single meteorite shower nearby the Thorsberg quarry about 470 Ma [*Alexeev*, 2010].

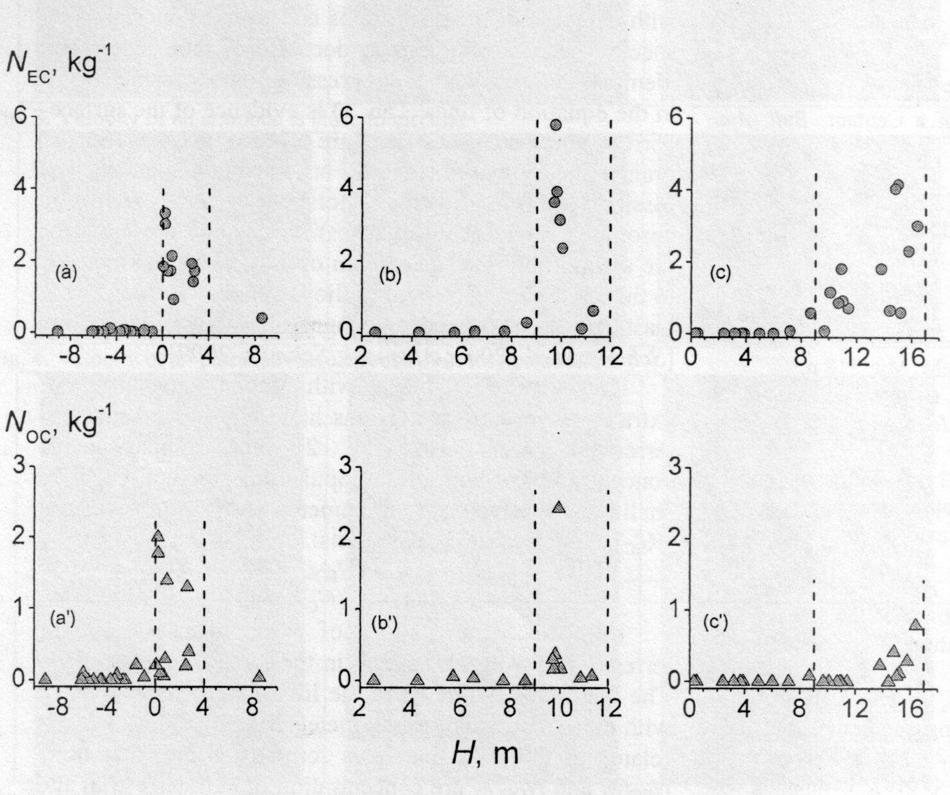

Fig. 2. Distribution of the extraterrestrial (a, b, c) and terrestrial (a', b', c') chromite grains in Ordovician limestone in the quarries of Sweden – Thorsberg + Hällekis (a, a'), Killeröd (b, b'), and China – Puxi River (c, c'). The *H* is a column depth. Dotted lines are marked the time intervals of the accumulation of sediments with fossil meteorites in the Thorsberg quarry. (According to [*Schmitz, Häggström*, 2006; *Häggström, Schmitz*, 2007; *Cronholm, Schmitz*, 2010].)

Table 2. Abundance of the extraterrestrial (EC) and terrestrial (OC) chromite grains in the quarries of Sweden (Thorsberg, Hällekis, Killeröd) and China (Puxi River). 1)

Quarry	Bed 2)	M, kg	N_{EC}	N_{OC}	N_{EC}/M, kg^{-1}	N_{OC}/M, kg^{-1}	K_{EC} 3)	K_{OC} 3)
Thorsberg &Hällekis	FM	173.9	332	142	1.91 ± 0.11	0.82 ± 0.07	49 ± 13	28 ± 9
	NFM	407.1	16	12	0.039 ± 0.010	0.029 ± 0.009		
Killeröd	FM	133.5	318	73	2.38 ± 0.14	0.55 ± 0.07	37 ± 12	42 ± 30
	NFM	153.4	10	2	0.065 ± 0.021	0.013 ± 0.010		
Puxi River	FM	165.3	283	25	1.71 ± 0.10	0.15 ± 0.03	26 ± 10	>5
	NFM	122.5	8	1	0.065 ± 0.023	<0.03		
All	FM	472.7	933	240	1.97 ± 0.07	0.51 ± 0.03	40 ± 8	23 ± 7
	NFM	682.9	34	15	0.050 ± 0.009	0.022 ± 0.006		

Notes:

1) According to [*Schmitz, Häggström,* 2006; *Häggström, Schmitz,* 2007; *Cronholm, Schmitz,* 2010];

2) FM и NFM – beds with and without fossil meteorites accordingly;

3) $K_{EC} = (N_{EC}/M)_{FM}/(N_{EC}/M)_{NFM}$; $K_{OC} = (N_{OC}/M)_{FM}/(N_{OC}/M)_{NFM}$. The values of K_{EC} and K_{OC} are factors of enrichment of limestone by extraterrestrial and terrestrial chromite grains respectively.

The study was financially supported according to Program No. 4 of the Presidium of RAS.

References

1. Alexeev V.A. (2010), Radiation history of fossil meteorites from Sweden, Solar System Research, 44, No. 4, 311-319.
2. Alwmark C., B. Schmitz (2009), The origin of the Brunflo fossil meteorite and extraterrestrial chromite in mid-Ordovician limestone from the Gärde quarry (Jämtland, central Sweden), Meteorit. Planet. Sci., 44, No. 4, 95-106.
3. Cronholm A., B. Schmitz (2010), Extraterrestrial chromite distribution across the mid-Ordovician Puxi River section, central China: Evidence for a global major spike in flux of L-chondritic matter, Icarus, 208, No. 1, 36-48.
4. Häggström Th., B. Schmitz (2007), Distribution of extraterrestrial chromite in Middle Ordovician Komstad Limestone in the Killeröd quarry, Scania, Sweden, Bull. Geol. Soc. Denmark, 55, 37-58.
5. Heck P.R., B. Schmitz, H. Baur, A.N. Halliday, R. Wieler (2004), Fast delivery of meteorites to Earth after a major asteroid collision, Nature, 430, No. 6997, 323-325.
6. Heck P.R., B. Schmitz, H. Baur, R. Wieler (2008), Noble gases in fossil micrometeorites and meteorites from 470 Myr old sediments from southern Sweden, and new evidence for the L-chondrite parent body breakup event, Meteorit. Planet. Sci., 43, No. 3, 517-528.
7. Meier M.M.M., B. Schmitz, H. Baur, R.Wieler (2010). Noble gases in individual L chondritic micrometeorites preserved in an Ordovician limestone, Earth Planet. Sci. Lett., 290, No.1-2, 54-63.
8. Schmitz B., Th. Häggström (2006), Extraterrestrial chromite in Middle Ordovician marine limestone at Kinnekulle, southern Sweden – Traces of a major asteroid breakup event, Meteorit. Planet. Sci., 41, No. 3, 455-466.
9. Schmitz B., Th. Häggström, M. Tassinari (2003), Sediment-dispersed extraterrestrial chromite traces a major asteroid disruption event, Science, 300, No. 5621, 961-964.
10. Schmitz B., B. Peucker-Ehrenbrink, M. Lindström, M. Tassinari (1997), Accretion rates of meteorites and cosmic dust in the Early Ordovician, Science, 278, No. 5335, 88-90

Barenbaum A.A.[1], Shpekin M.I.[2] About age of the lunar surface

[1] Oil and Gas Research Institute RAS; [2] Kazan university
azary@mail.ru ph(499) 135-72-21;
Michael.Shpekin@ksu.ru ph (843) 292-77-97

Key words: Planets, craters, galactic comets, volcanic and tectonic processes.

Abstract Most part of the lunar surface relief was formed during the last 5 *Ma*. This conclusion was received on the basis of detail analysis of large craters of the Moon, Earth, Mars and Mercury. Falling of the galactic comets in the period 5÷0.6 *Ma*, and the tectonomagmatic processes induced by the comets falling played major role in shaping of the Moon topography. Processes of tectonics and volcanism are occurring on the Moon today also. We found volcano in the Tsiolkovsky crater on the reverse side of the Moon that can serve as good example of that. The volcano has a height of 102 *m* and is located almost in the bottom center of the crater with a diameter of 180 *km* on a low oval elevation of plume nature 24-26 *km* in size.

Introduction It is believed that the relief of the lunar surface, as well as Mercury and Mars have formed more than 3000 *Ma* as a result of falls on these celestial bodies planetesimals that remained in the interplanetary space after the Solar system formation [*Hiesinger et al.*, 2010]. To substantiate this view are used data on the craters, as well as measurements of the isotopic age samples of lunar rocks delivered to Earth and testifying to their formation more than 3000 *Ma* [*Hayes, Walker*, 1975]. The planetary exploration by spacecraft made in recent years, however, cast doubt on such an ancient age of the surface topography, in particular, the Moon and Mars. Large masses of frozen water were discovered at the poles this celestial bodies. Moreover recently dry riverbeds can be seen on the Mars [*Wikipedia*]. These and many other facts do not find a convincing explanation within the framework of existing concepts.

We suggest another interpretation of the observed facts. It is based on attracting galaxycentric paradigm [*Barenbaum*, 2010] to analyze the distribution a cometary craters on surface planets as well as on the discovery in one of them (in the Tsiolkovsky crater on the reverse side of the Moon) modern volcano [*Shpekin*, 2009]. Our studies show that most of the surface of the Moon, Mars and Mercury are completely saturated by such craters. Owing to that formation the craters is associated with ejection of rocks from depths of ~ 3 *km* or more large age of the lunar rocks samples says in the first place about the time of solidification of their material but not about the actual age of the formation of the lunar surface.

Below we present arguments and evidence that the age of lunar surface is hardly older 5 *Ma* and the process formation of surface the Moon continues today.

General characteristics of the Moon relief The main topographical features of the topography of the Moon, Mars and Mercury are uplifted the areas of surface – "continents" and the more lower areas of the surface – "seas". Continents uninterruptedly dotted with large craters, while the seas covered by craters to a much lesser degree. It is significant that the continents tend to be located the southern hemisphere of the celestial bodies whereas marine surfaces is mainly located in its northern hemisphere.

There is also an important specificity in the morphology and distribution of craters. According to [*Pike*, 1977] on the moon we can distinguish two different populations of craters – with a diameter $D < 15$ *km*, and with $D > 15$ *km*. The first are the most numerous in the seas, and the second – on the continents. The depth H of the first is approximately equal to 1/5 of their diameter, while depth craters of the second type is smaller. The first type of craters has a simple structure and is best described by the dependence $H = 0.196\ D^{1.01}$, whereas the second type is more complicated. The second type craters has central hills and gentle slopes. In the diameter range from 11 to 400 *km* these craters are followed the depending $H = 1.044D^{0.301}$. Thus in the process of impact origin craters on the surface may be ejected rocks from a depth of ~3÷7 *km*.

The transition between the types of craters on the curve H(D) is not monotonic, forming a region of overlap. The same applies to craters on the Mars and the Mercury [*Melosh*, 1989].

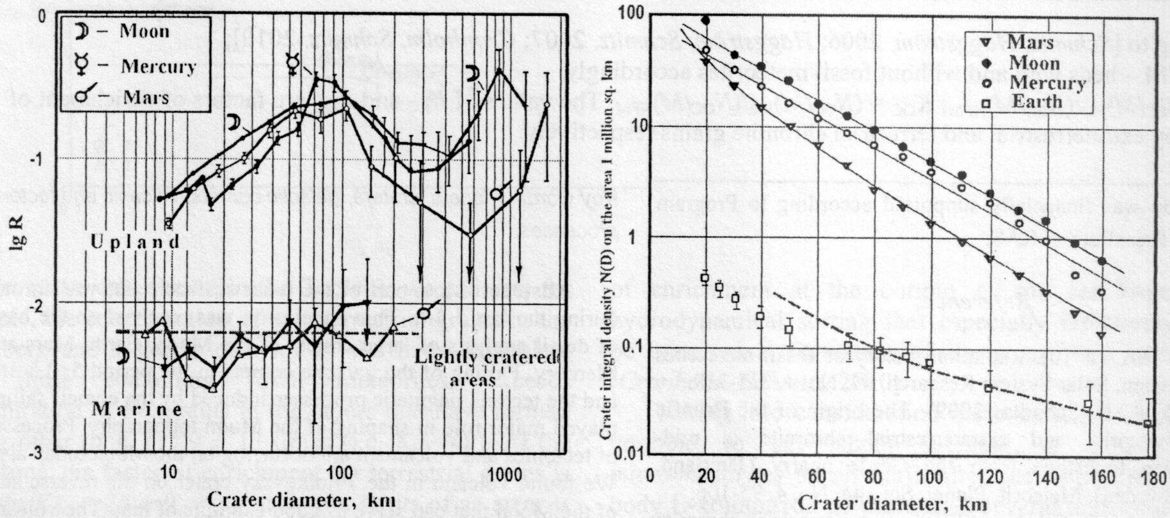

Fig. 1. Density distribution of craters by diameter: a) the differential N(ΔD) with a step $\Delta D = D \div \sqrt{2}D$ in a double logarithmic scale [*Voronov et al*, 1986], and b) the integral N(>D) in a logarithmic scale [Barenbaum, 2010], constructed according to data [*Kazimirov et al*, 1980]. The dotted line in the figure corresponds inversely quadratic dependence on D.

The distributions of craters by diameter as well as their density on the continents and in seas are also turn out peculiar (Fig. 1-a). For craters with D ~100 *km* their density on the continents is 100 times higher than in the seas, and at D ~10 *km* this difference is reduced to ~10. Significant differences in the density craters on different planets appear only for $D > 400$ *km*, where the density of craters on the Moon in 4-10 times higher than on the Mars.

The distributions craters of the Moon, the Mars and the Mercury are similar in configuration and are close in numerical parameters. Since the last craters are more numerous the exponential distribution of craters by diameter is intrinsic for these planets in general (Fig. 1-b).

Bending curves in Fig. 1-a for the continents at D = 60÷100 *km* and line graphs for the seas are explained by two [*Voronov et al*, 1986] or even by three [*Urey*, 1975] space bodies bombardments of different ages that that partially destroyed the traces of more early fallings. Modeling the distribution of craters by means of special selection of sizes cosmic bodies [*Voronov et al*, 1986], however, is not allowed to conclusively resolve this question [*Melosh*, 1989].

It is more difficult to explain [*Marov*, 1981] similarity in the distribution of craters in so much different celestial bodies like the Moon, Mars and Mercury that are differ by its geological history, the force of gravity on the surface and the distance from the asteroid belt and the Sun. The basic idea for explaining is associated with the possibility of complete saturation of large craters at least the surface of the continents [*Gault*, 1970; *Basilevsky*, 1977; *Woronov*, 1977; *Voronov et al*, 1986]. This problem was not resolved. Currently accepted view is [*Melosh*, 1989] that planets are far from the state of saturation by the large craters.

A new approach to the problem According to [*Barenbaum*, 2010] the Sun in its motion in the Galaxy once in every 20-37 *Ma* is crosses the jet streams of substance flowing from the center of our star system. In moments of these intersections duration ~2÷5 *Ma* the Solar system is exposed to intense bombardments by galactic comets. In the Earth's geological history all these times are marked as the eras of global natural catastrophes. These events are accepted as the boundaries straton of modern geochronological scale.

Last bombardment by galactic comets occurred in the period 0.6÷5.0 *Ma* at the boundary of the Neogene and the Quarter [*Barenbaum et al*, 2002]. Today these comets are absolutely unavailable for detection from the Earth by means of astronomy. Therefore we are judging about the properties of these objects proceeding from the consequences of their falling on our and other planets, as well as the results of their collisions with a bodies of the asteroid belt [*Barenbaum*, 2010].

Available data suggest that the masses of the nuclei of galactic comets are varied in the range from 10^{12} to 10^{17} *g* and their kinetic energy is varied from 10^{20} to 10^{25} *J*. The

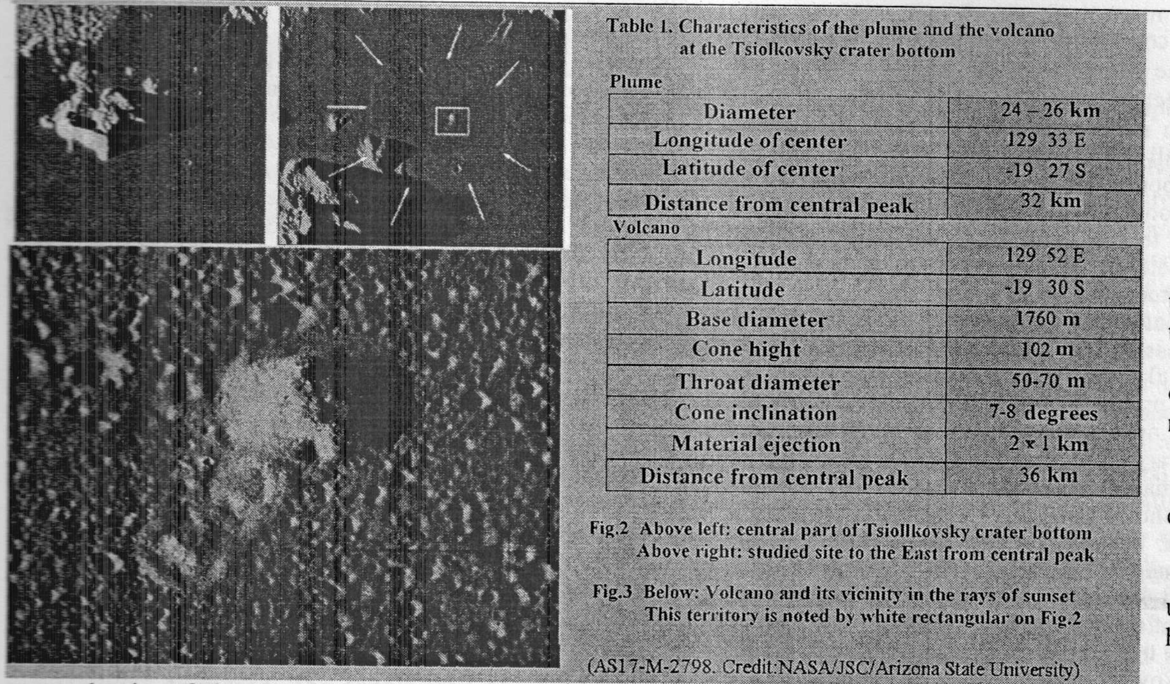

Table 1. Characteristics of the plume and the volcano at the Tsiolkovsky crater bottom

Plume

Diameter	24 – 26 km
Longitude of center	129 33 E
Latitude of center	-19 27 S
Distance from central peak	32 km

Volcano

Longitude	129 52 E
Latitude	-19 30 S
Base diameter	1760 m
Cone hight	102 m
Throat diameter	50-70 m
Cone inclination	7-8 degrees
Material ejection	2 × 1 km
Distance from central peak	36 km

Fig.2 Above left: central part of Tsiollkovsky crater bottom
Above right: studied site to the East from central peak

Fig.3 Below: Volcano and its vicinity in the rays of sunset
This territory is noted by white rectangular on Fig.2

(AS17-M-2798. Credit:NASA/JSC/Arizona State University)

matter density of the comet is close to 1.0 g/cm^3. It is composed of 80-90% water ice and of ~10-15% the carbonic component. Chemical elements heavier than carbon and oxygen are possessed by space prevalence. Their content is not more than one percent [*Barenbaum*, 2010].

The falls of galactic comets are characterized as "cometary showers" when during one bombardment $\sim 10^4 \div 10^7$ such bodies could fall on the Earth. In contrast to large asteroids and comets of solar system these comets are characterized by an exponential distribution of mass and energy that causes the same distribution of diameters of the craters created by them (Fig. 1-b).

At the same time the number of the falling comets is so great that full saturation of the surface by craters is reached even during one bombardment period. The theoretical value of the "ultimate" density of the craters for the Moon, Mars and Mercury is ≈100 craters with a diameter $D \geq 10$ *km* on area 1 million km^2 [*Barenbaum*, 2010]. Because of the obliquity of the ecliptic at an angle of 62° to the galactic plane in which occur comets moving, their latest bombardment came mainly to the southern hemisphere of the planets. Thus the complete saturation of the craters exists only in that hemisphere of the Moon and the Mars. Data in Fig. 1-b confirm this conclusion.

There is another important fact that should be noted in discussing the data of Fig. 1-b. This is the absence of craters on the Earth, created by galactic comets. All the large craters on Earth are formed owing to asteroids downs. The distribution diameter of these craters by in region $D \geq 70$ *km*, slightly garbled observational selection, well described by inversely quadratic dependence.

The facts and calculations suggest that fragile nuclei of galactic comets are inevitably disintegrated in the atmospheres of the Earth and the Venus. In result raises the powerful hypersonic jet [*Barenbaum and Shuvalov*, 2007], which does not create a crater and the whole enormous kinetic energy of the comets is directed to heating and melting of the rocks up under the surface planet. Subsequently, this energy is released in different tectonic and volcanic processes [*Barenbaum et al*, 2004]. Typical manifestations of these processes [*Barenbaum*, 2008] in a "thin layer" lithosphere are the formation of seamounts on the Earth, and shield volcanoes on the Venus, whereas in case "powerful" lithosphere takes place the so called phenomenon of "newest raisings". This phenomenon consists in almost synchronous uplift of the half surface area continents of the globe at the past 5 *Ma*. Different geological structures have tested significant rise during this period. Among them: the Antarctic continent; most part of Africa; the Central and North-Eastern Asia; the Western North and South America; Guiana and Brazilian shields; the Scandinavian Mountains; the Greenland; the Urals; the Siberian platform; the Alps and other structures [*Artyushkov*, 1994].

The lifting height was different. On most of the Pacific coast, she was the first hundreds of meters, on the Siberian platform ~200-1000 *m*, in South Africa ~300-400 *m* in the west and ~900-1200 *m* in the east. The fastest growth occurred in mountainous terrain. For example the Arabian platform increased the height of 2 *km*, the Alps – up to 3 *km*, and the Himalayas – up to 6 *km*. The rising of asthenosphere is observed under most of the mountains. In separate flat sections the lift leads to the uplift of crystal blocks in diameter ~ n(10-100) *km* to a height of up to ~1 *km* at distance between the elevations greater than their diameter. In some places rising of asthenosphere was accompanied by modern intense outpourings of magma [*Artyushkov*, 1994].

Similar processes occur on the Mars. Calculations show that even ~100 times less dense than on the Earth, its atmosphere leads to two important physical effects. On the one hand, it causes severe ablation of the galactic nuclei of comets, which reduces the diameter of a crater and shifts the distribution in Fig. 1-b relative to the Moon. And on the other hand, the part of comet's energy goes into heating asthenosphere under the southern hemisphere of Mars, It is explains uplifting of southern hemisphere of Mars on 2-4 *km* relatively flat northern hemisphere which has much less craters. Huge volcanoes of the Mars, with clear indexes of recent activity are probably the channels of excess heat from the asthenosphere of the planet.

Volcanic and tectonic processes have occurred on the Moon in last 5 million years albeit on a smaller scale. They continue today.

Modern volcano-tectonic processes on the Moon

Many researchers mark the evidences of such processes in form craters filled by caked lava with inclined surface as well as craters destroyed by deep rifts. In 1958 Kozyrev [1959] established on the Moon volcanic activity is directly. He found small emission of volcanic ash and gas in the Alphonsus crater with a diameter of 120 *km* on the visible side of the Moon. Spectral analysis showed the presence in the ejection of molecules C_2, CN, etc.

Another, even more compelling example of volcanic processes is a small volcano [*Shpekin*, 2009]. The volcano is located at the bottom of the Tsiolkovsky crater on the far side of the Moon and was discovered on the basis of images delivered to the Earth by "Apollo-17" mission. Crater has a diameter of 180 *km*. He is characterized by a complicated structure and by existence the central peak, typical for craters of cometary origin.

The volcano is located almost in the center of the crater on a small flat oval raising by diameter 24-26 *km*. This raising very probably has nature of plume. On high-resolution images are visible lava flows, indicating about almost contemporary eruption of the volcano (Fig. 3).

Estimates made on the basis of images photogrammetry showed that the height of the volcano is about 102 meters. Diameter at the base of the volcanic cone is 1,760 meters. Slopes of the volcano have an inclination toward the bottom of the crater on angle about 7-8°. Emissions of the material are observed only in one direction and this trend points to the central peak on the bottom of Tsiolkovsky crater. Other characteristics are listed in Table 1 [*Shpekin*, 2009; *Shpekin and Barenbaum*, 2011].

Several small craters we can see at the top of the cone if closer to look in Fig.3. It is probably the canals through which volcanic material in form of lava turns out on lunar surface. The diameter of the central conduit is about 50-70 meters. Volcanic cone contains no small impact craters that indicating at its young age. Reflective properties of the volcano say about the same. The surface of cone volcano is noticeably brighter than the surrounding terrain, because it had not yet covered with dark lunar dust. This evidence supports our conclusion that volcanic activity ended or recently, or perhaps it even has a modern character.

It is significant that the volcano is located in the center of the small sublime structure of tectonic-magmatic nature. Such combination of both geological objects on the Earth is typical for shallow "magmatic chambers" that arise under planet surface into the place of galactic comet falling [*Barenbaum*, 2010a]. Very probably such magmatic chamber has arisen and exists today under the bottom of the Tsiolkovsky crater.

Summary and conclusions

- The time of formation of the main topographic structures (continents and seas) on the Moon as well as all the planets are not uniquely associated with the age of rocks composing these structures.
- The main factor that determined the modern look of the Moon, Mars and Mercury was the bombardment of the solar system by galactic comets between 5-0.6 *Ma*.
- Mass fallings of galactic comets are causes of abrupt activization of tectonic and volcanic processes that continue on the Moon and planets to this day.
- An example of these processes is discovery at the Tsiolkovsky crater, apparently, an active volcano 102 meters high, locating on a low plume base with diameter of 24-26 *km*.

In this regard it should be emphasized that the questions formation of the "Geodynamic Camera" located under large impact craters still have not been studied theoretically [*Barenbaum*, 2010b].

References

1. Artyushkov E.V. (1994) The newest uplifts of terrestrial crust on continents as consequences of lifting of great hot matter masses from the mantle // *Doklady Akad. Nauk, V.*336, №5, p.680-683 (in Russian).
2. Basilevsky A.T. (1973) Distribution of lunar craters over sizes // *Space Researches V.11* (4), p.612-622 (in Russian).
3. Barenbaum A.A. (2008) Processes in the Earth crust and upper mantle: problems of the mountain building and the newest terrestrial crust elevation *//Connection between surface structures of the terrestrial crust with deep-seated ones*, Materials XIV Intern. Conference. Petrozavodsk, Karelian Science Center RAS, P.1, p.43-47 (in Russian).
4. Barenbaum A.A. (2010) *Galaxycentric paradigm in geology and astronomy*, Moscow: BH LIBROKOM, 544 p. (in Russian).
5. Barenbaum A.A. (2010a) A possible mechanism creating of dyke complexes by galactic comets // *Proceedings of XLIII meeting on the Tectonics: Tectonics and Geodynamics of the fold belts and Phanerozoic platforms*, V.1. Moscow. PH GEOS, p.38-42 (in Russian).
6. Barenbaum A.A. (2010b) Modeling of falling to the ground of large cosmic bodies. Testing according to data of geology. Unresolved issues // *Zababakhin readings: Proceedings of the X Intern. Conference*. Snezhinsk. PH VNIITF. p.13 (in Russian).
7. Barenbaum A.A, Yr.B. Gladenkov, N.A. Yasamanov (2002) Geochronological scale and astronomical time // *Stratigraphy. Geological Correlation. V.10.* № 2. p.3-14. (in Russian).
8. Barenbaum A.A., V.E. Hain, N.A. Yasamanov (2004) Large-scale tectonic cycle: an analysis from the standpoint of the galactic concept // *Vestnik MGU. Ser.4. Geology.* № 3. p.3-16.
9. Barenbaum A.A., V.V. Shuvalov (2007) Modeling the interaction of galactic comets with the atmosphere // *Physics extreme states of matter-2007*, Ed. Fortov V.E. etc., Chernogolovka: IPCP. p.139-140 (in Russian).
10. *Wikipedia*. http://ru.wikipedia.org/wiki/Mars_(planet)
11. Voronov A., R.G. Strom, M.Garkis (1986) Interpretation of crater chronicles: from Mercury to Ganymede and Callisto // *Satellites of Jupiter*, Moscow: Mir, Part 2. p.5-48 (in Russian).
12. Kazimirov D.A., B.D. Sitnikov, G.A. Poroshkova and others (1980) *The density distribution of craters on the Moon, Mercury and Mars.* Preprint GIN-GAISH (in Russian).
13. Kozyrev N.A. (1959) Volcanic activity on the Moon // *Priroda.* № 3. p.84-87 (in Russian).
14. Marov M.Ya. (1981) *Solar system Planet.* Moscow: Nauka (in Russian).
15. Melosh H.J. (1989) *Impact Cratering. A Geologic Process.* Oxford. Oxford Univ. Press.
16. Hays J.F., J. Walker (1975) Igneous lunar rocks // *Cosmochemistry Moon and planets.* Ed. Vinogradov A.P., Moscow. Nauka. p.274-282 (in Russian).
17. Shpekin M.I., A.A. Barenbaum (2011) On the nature of the endogenous activity in the crater Tsiolkovsky on the Moon // *Proceedings of the conference VNKSF-17.* Ekaterinburg. p.476-477 (in Russian).
18. Urey G. (1975) Origin of the Moon and Solar System // *The Moon,* Eds. Runcorn S. and Urey H. Moscow. Mir. p.287-302 (in Russian).
19. Gault D.E. (1970) Saturation and equilibrium conditions for impact cratering on the lunar surface. Criteria and implications // *Radio Sciences. V.5.* p.273-291.
20. Hiesinger H., J.W. Head III, U. Wolf, R. Jaumann, G. Neukum (2010) Ages and stratigraphy of lunar mare Frigoris and other nearside maria based on crater size-frequency distribution measurements // *J. Geophys. Res. V.115,* E03003, doi: 10.1029/2009JE003380.
21. Pike R.J. (1977) Size-depend in the shape of fresh impact craters on the Moon // *Impact and explosion cratering*, Eds. Roddy D., Pepin R., Merrill R., Pergamon Press. New Work. p.489-509.
22. Shpekin M.I. (2009) The Last «Apollo» Orbit Pass over the Tsiolkovsky Crater // *Intern. Conf.: Astronomy and World.*

Heritage: Across Time and Continents. Kazan. Russia. p. 219-221. http://www.ksu.ru/f6/ k8/bin_files/ols138.pdf.

23. Woronov A. (1977) Crater saturation and equilibrium: A Monte Carlo simulation // *J. Geophys. Res., V.82*, p.2447-2456

Egorov V.K.[1], Egorov E.V.[1], Kashkarov L.L.[2], Polukhina N.G.[3] X-ray and ion beam study of natural olivine $(Mg_{1-x}Fe_x)_2SiO_4$

[1]Institute of microelectronics technology of the Russian Academy of Sciences, Chernogolovka; Egorov@iptm.ru

[2]Institute of geochemistry and analytical chemistry of V.I. Vernadsky of the Russian Academy of Sciences, Moscow

[3] Physical institute of P.N. Lebedev of the Russian Academy of Sciences, Moscow

The short characteristic of crystallographic and physical properties of olivines is presented, and also some features of the experimental methods used for their testing are discussed. The element composition and structure perfection for group of natural olivines with various geneses were diagnosed. The simple way of the natural olivine analysis by X-ray diffractometry method of the olivine textures produced owing to the magnitocrystalline anisotropy of these crystals is offered.

The mineral with name olivine represents a solid solution $(Mg_{1-x}Fe_x)_2SiO_4$ which extreme members have the name forsterite (Mg_2SiO_4) and fayalite (Fe_2SiO_4). Interest to properties and features studying of this mineral is caused by that it is the rock-forming component of the Earth upper mantle and simultaneously represents one of two basic phases forming iron-stony meteorites-pallasites [*Willie*. 1971]. In particular, the comparative analysis of admixture composition and degree of the crystal structure imperfection for olivines with different composition and origin history allows to hope for use of this mineral as the independent detector of particles energy and its atomic weight in cosmic radiation streams.

Olivine group D_{2h}^{16} - P_{bnm} concerns to the rhombic system. Lattice constants of this mineral vary from values a_1=0.4762 nm, b_1=1.0225 nm, c_1=0.5994 nm, corresponding forsterite, to sizes a_2=0.4815 nm, b_2=1.0466 nm, c_2=0.6099 nm, peculiar fayalite. The element composition variation allows to estimate intervals of parameters change featured for a olivine crystal lattice: Δa=0.0053 nm, Δb=0.0241 nm, Δc=0.0105 nm. Structural motive of olivine crystals formation is a hexagonal close-packed array atoms of oxygen (ABAB) with existence of some distortions. Layers are packed along "a" crystallographic axis. That is the reason why the change of this lattice parameter at transfer from Mg_2SiO_4 to Fe_2SiO_4 is smallest. Coordination number of the structure is z=4. At the element composition change from Mg_2SiO_4 to Fe_2SiO_4 the crystal density of olivines varies from 3.2 to 4.4 g/sm^3. Mg_2SiO_4 is colourless. Replacement of Mg on Fe atoms leads to occurrence of a greenish shade, and at considerable concentration of iron - to change of colour to brownish-black. The farsterite crystals interaction with a magnetic field shows diamagnetic behaviour. At Fe atoms appearance in the structure olivine transforms it into paramagnetic anisotropy state. For example, the magnetic susceptibility of $(Mg_{0.98}Fe_{0.02})_2SiO_4$ has values $\chi_c=77.2\cdot10^{-6}$; $\chi_b=58.2\cdot10^{-6}$; $\chi_a=56.9\cdot10^{-6}$ [*Ferre*. 2005]. Experimental investigations show, that for all olivine compositions the next relation $\chi_c>\chi_b\cong\chi_a$ is right.

This work presents the results of experimental investigations of olivines a terrestrial and space origin by methods a X-ray diffractometry, TXRF spectrometry [*Klockenkamper*, 1997] and ion beam analysis [*Chu and all*, 1978]. X-ray diffractometry measurements were carried out with use HZG-4 digital goniometer in conditions of the standard focusing geometry, using symmetric and asymmetrical geometry of an analyzing sample installation. The asymmetrical geometry application is the important experimental means for study of monocrystals when their external surface is not parallel to the crystallographic planes chosen for analysis. TXRF measurements were carried out as with use the special TXRF cell, and on base of the digital goniometer application in the conditions of sliding falling of X-ray primary exciting beam. In both cases X-ray exciting beam was formed by means of a quartz wave guide-resonator.

The ion beam testing of olivine samples has been executed on the ion beam analytical complex Sokol-3 by Rutherford backscattering (RBS) He^+ and H^+ ions with energy $E_0\approx1.5$ MeV.

Figure 1 shows TXRF spectrum of $(Mg_{0.88}Fe_{0.12})_2SiO_4$ olivine monocrystal having a terrestrial origin. The orientation of its reflecting surface has (0k0) configuration. The spectrum is characterized by a low intensity of the background component and is free from matrix effects. He allows to estimate the relative content in the sample of matrix elements Si and Fe and concentration of basic impurities (Ca and Mn). At the same time, despite the highest sensitivity of TXRF spectroscopy the spectrum does not allow to estimate adequately the content of all matrix elements featured for olivine structure. Such estimation can be carried out on the basis of RBS spectra approximation. Figure 2 presented RBS experimental spectra of He^+ and H^+ collected for case of the olivine crystal random orientation. On inserts the geometry of measurements is shown. Detailed approximation of spectra has shown, that the composition of the sample corresponds to $(Mg_{0.93}Fe_{0.07})_2SiO_4$.

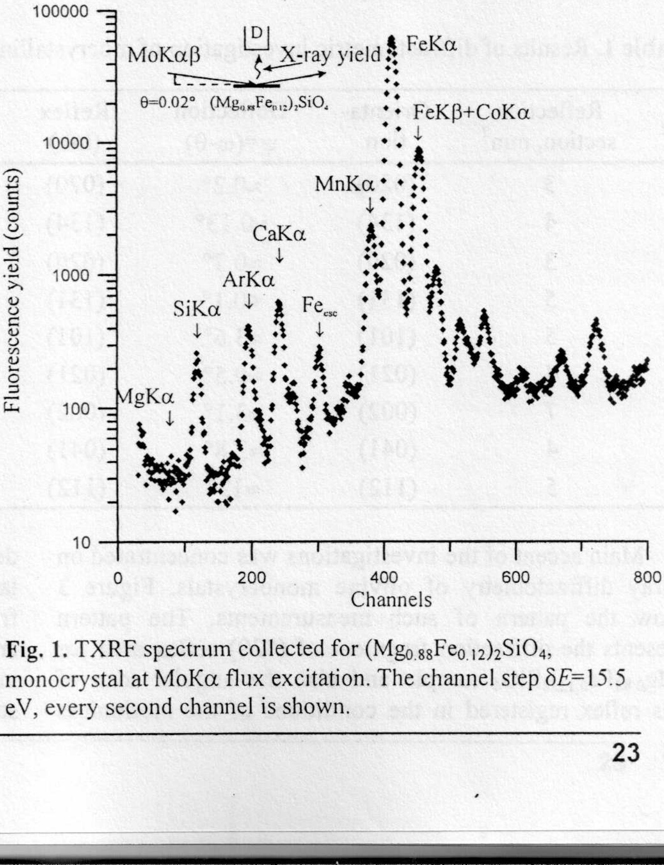

Fig. 1. TXRF spectrum collected for $(Mg_{0.88}Fe_{0.12})_2SiO_4$, monocrystal at MoKα flux excitation. The channel step δE=15.5 eV, every second channel is shown.

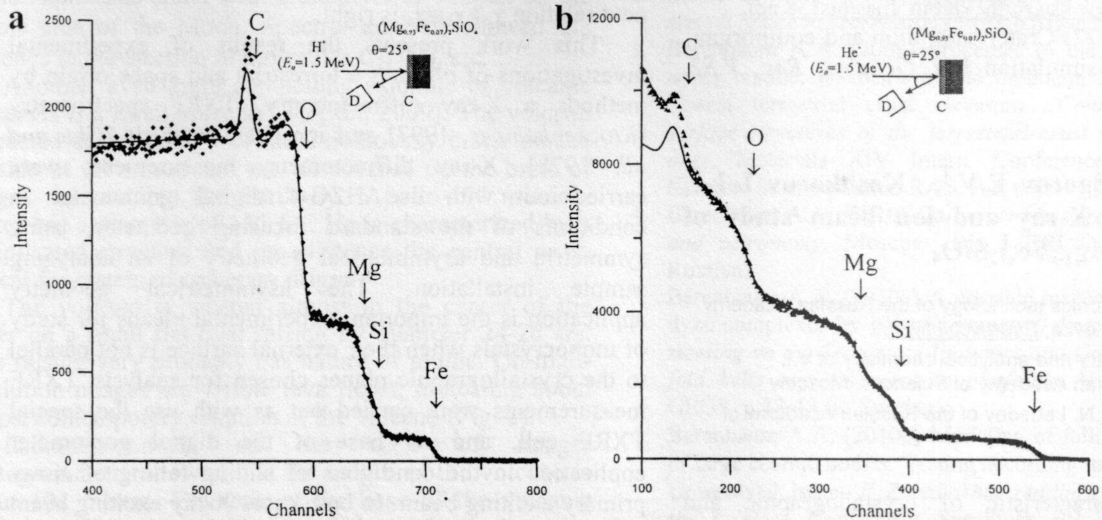

Fig. 2. RBS spectra of He^+ and H^+ collected for random oriented and mechanical polished $(Mg_{0.93}Fe_{0.07})_2SiO_4$ monocrystal. On the sample surface the carbon film with thickness near 20 nanometers is observed. The channel step δE=1.9 keV, every third channel is shown.

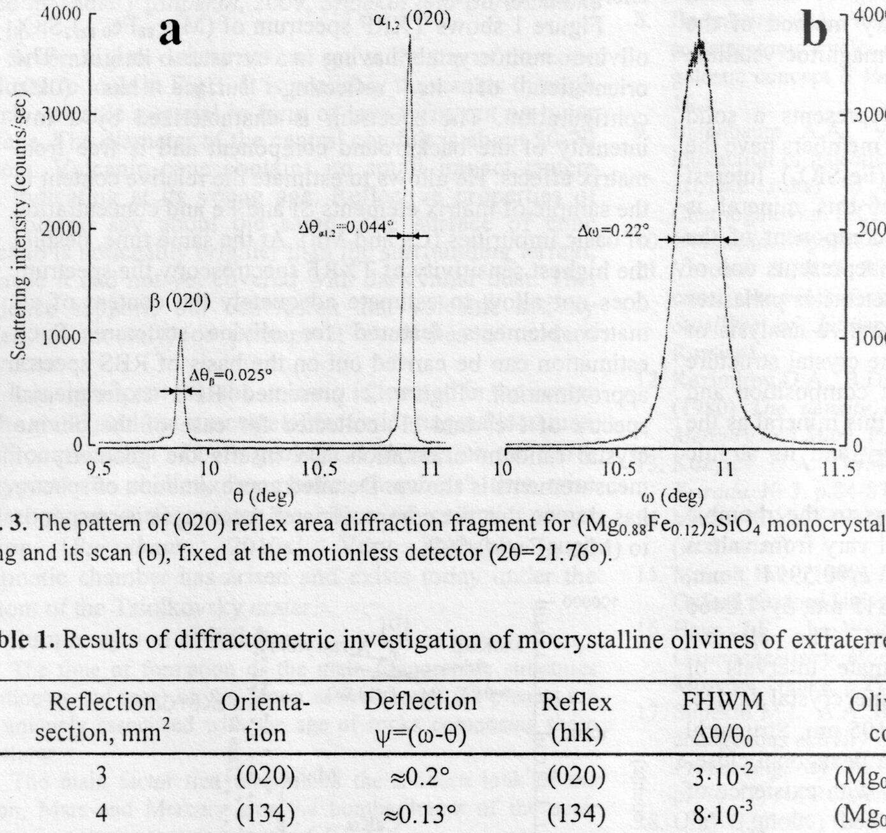

Fig. 3. The pattern of (020) reflex area diffraction fragment for $(Mg_{0.88}Fe_{0.12})_2SiO_4$ monocrystals received with FeKαβ (a) radiation using and its scan (b), fixed at the motionless detector (2θ=21.76°).

Table 1. Results of diffractometric investigation of mocrystalline olivines of extraterrestrial origin.

№	Reflection section, mm^2	Orienta-tion	Deflection ψ=(ω-θ)	Reflex (hlk)	FHWM $\Delta\theta/\theta_0$	Olivine element composition	Crystallinity level
1.	3	(020)	≈0.2°	(020)	$3\cdot10^{-2}$	$(Mg_{0.84}Fe_{0.16})_2SiO_4$	low
2.	4	(134)	≈0.13°	(134)	$8\cdot10^{-3}$	$(Mg_{0.88}Fe_{0.12})_2SiO_4$	middle
3.	3	(020)	≈0.7°	(020)	$4\cdot10^{-2}$	$(Mg_{0.84}Fe_{0.16})_2SiO_4$	high
4.	5	(131)	<0.1°	(131)	$1\cdot10^{-3}$	$(Mg_{0.91}Fe_{0.09})_2SiO_4$	high
5.	5	(101)	≈3.6°	(101)	$1\cdot10^{-3}$	$(Mg_{0.88}Fe_{0.12})_2SiO_4$	high
6.	4	(021)	≈0.5°	(021)	$2\cdot10^{-3}$	$(Mg_{0.93}Fe_{0.07})_2SiO_4$	middle
7.	7	(002)	≈3.1°	(002)	$1.3\cdot10^{-3}$	$(Mg_{0.86}Fe_{0.14})_2SiO_4$	texture
8.	4	(041)	≈3.8°	(041)	$1\cdot10^{-3}$	$(Mg_{0.92}Fe_{0.08})_2SiO_4$	high
9.	5	(112)	≈13°	(112)	$6\cdot10^{-3}$	$(Mg_{0.94}Fe_{0.06})_2SiO_4$	middle

Main accent of the investigations was concentrated on X-ray diffractometry of olivine monocrystals. Figure 3 show the pattern of such measurements. The pattern presents the diffraction fragment of (020) reflex area for $(Mg_{0.88}Fe_{0.12})_2SiO_4$ sample and also the angular scan of this reflex registered in the conditions of the motionless detector. Values of FWHM for both sections of reciprocal lattice point, which actually represent the shown fragments, allows to expect rather high perfection of a crystal lattice olivine a crystal. At the same time, RBS measurements executed in parallel with the diffraction study have not shown channeling ion effect for this crystal.

In addition to study of terrestrial origin olivines the group of olivine monocrystals extracted from stony-iron meteorites (pallasites) has been analyzed. Results of these investigations are resulted in the table. The table shows, that the olivine element composition is grouped about two concentration positions: $(Mg_{0.93}Fe_{0.07})_2SiO_4$ and $(Mg_{0.86}Fe_{0.14})_2SiO_4$. Available data do not allow to connect the olivine composition with level of its monocrysallinity. Unfortunately, the smallest sizes of there crystals have not allowed to execute ion beam testing for them.

Additional field meant in the work, is connected with the magnetic textures allowing rather easily to classify polycrystalline and powder olivine fractions on size of lattice parameter "c". As it has been noted above, the magnetic susceptibility of paramagnetic olivines demonstrates maximum along an axis "c", that allows to build the crystalline texture in a magnetic field with enough value induction, fixing the textures in tablets of epoxy sealant. Figure 4 shows patterns, received for $(Mg_{0.93}Fe_{0.07})_2SiO_4$ of a terrestrial origin in conditions of texturing and random distribution of its polycrystalline fraction. The diffraction fragment of the texturing fraction demonstrates (00l) type reflexes only, and intensities of the peaks are incomparably above of intensities corresponding to the reflexes which are characterized the pattern of the random sample. The angular evolvent of (004) reflex shown on the insertion allows to differ the olivine monocrystal from the texture ensemble. In the result, the using of olivine textures in many cases can facilitate interpretation of geological breeds genesis by such way of the olivine fractions diagnostics.

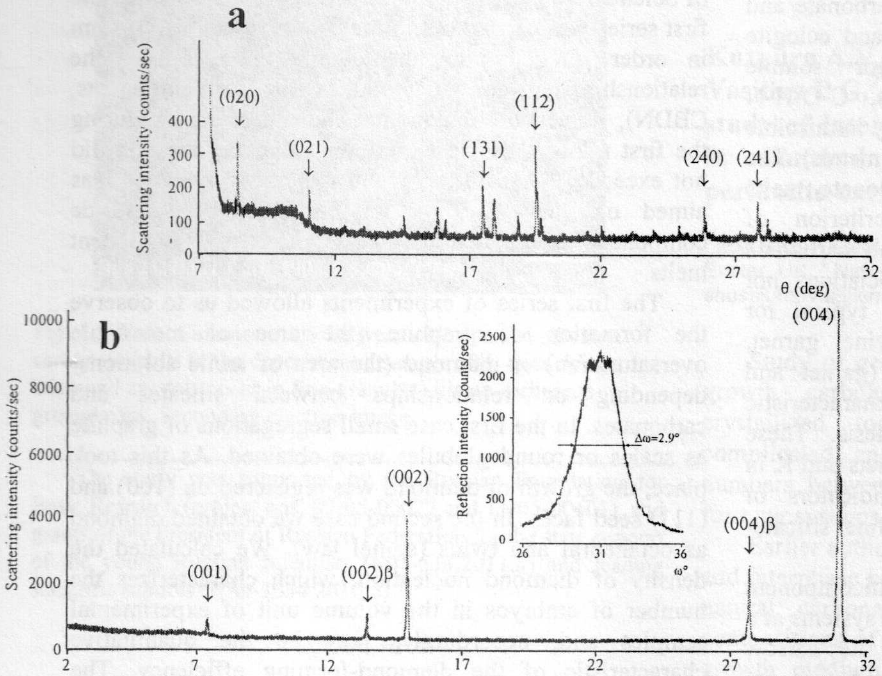

Fig. 4. Patterns of $(Mg_{0.93}Fe_{0.07})_2SiO_4$ olivine samples collected by using of CuKα radiation for the polycrystal ensemble with its random orientation (a) and in condition of the texture state with (00l) primary orientation (b). The insertion presents the (004) reflex angular evolvent collected in condition of the detector position (2θ=61.82°).

References

1. Chu W.K., Mayer J.M., Nicolet M.A. (1978), *Backscattering Spectrometry*. New York: *Academic Press*, 384 p.
2. Ferre E.C. (2005) *Tectonophysics, 398*. 141-166.
3. Klockenkamper R. (1997), *Total Reflection X-ray Fluorescence Analysis. New York: Wiley*, 245 p.
4. Willie R.J. (1971), *The Dynamic Earth: Textbook on Geoscience. New York: Wiley*, 416 p.